Secular resonance transitions in the late Cretaceous and astronomical imprints during the Oceanic Anoxic Event II (Schill Grund Platform, North Sea, Offshore Netherlands)

M. Arts[1*], A.C. Da Silva[1], G.J. Vis[3], D. Beelen[4] F.J. Hilgen[2]

1Universite de Liège, Department of Geology, Sedimentary Petrology

Allée du Six Aout 12, 4000, liège, Belgium

2 Utrecht University, Department of Earth Sciences, Stratigraphy & paleontology

Vening Meineszgebouw A, Princetonlaan 8,3584 CB Utrecht, The Netherlands

3 TNO Geological Survey Netherlands

Princetonlaan 6, 3584 CB Utrecht, the Netherlands

4 Utrecht University, Department of Physical Geography

Vening Meineszgebouw A, Princetonlaan 8,3584 CB Utrecht, The Netherlands

E-mail addresses `Michiel.arts@uliege.be` (M. Arts)

Abstract

The Chalk Group deposited on the Schill Grund Platform in Dutch offshore comprises a near complete early Danian to late Cenomanian chalk succession. Such a long record (~30 Myrs) allows for the study of long period (>1 Myr) astronomical cycles providing insights into amplitude modulation of astronomical cycles. A 405kyr eccentricity-based tuning was created for one gamma-ray log and one thorium well-logs which go through the Chalk Group. These results were tuned to astronomical solution La2010d, which were then be used to study aspects of long period astronomical cycles. Firstly, the amplitude modulation of the 405 kyr eccentricity by long period astronomical cycles was studied, which indicates that secular resonance transitions took place at ~85 Ma and ~92 Ma. The secular resonance transition at ~92Ma shifted the duration of the 2.4 Myr eccentricity cycle to a 1.2 Myr period while the resonance transition at ~85 Ma shifted the period shifted back 2.4 Myr. The amplitude modulation records were also compared to the amplitude modulation records of astronomical solutions. None of the astronomical solutions accurately model the observed resonance transition. The second result is related to Ocean Anoxic Event II (OAEII). The 2.4 Myr cycle is at a maximum ~ 400kyr before the onset of OAEII and progressively transitions towards a minimum during OAEII, as the 1.2 Myr obliquity cycle peaks during OAEII. This phase relationship between these astronomical cycles leads to a progressive increase in the contribution of the obliquity to the astronomical-insolation signal during OAEII.

1. Introduction

The development of the Astronomical Time Scale is one of the great advances in modern geochronology. Cyclic variations in the Earth's orbit and tilt relative to the Sun (commonly known as the Milankovitch Cycles), influence Earth's climate, which is recorded in the sedimentary record as equally cyclic changes in the stratigraphy. Cyclic sediments act as a geological 'clock' and can thus be used to create timescales based on numerically calculated solutions for the different astronomical cycles. The geological timescale has been astronomically calibrated in such a way down to the Middle Jurassic (Huang, 2018). On top of the precession, obliquity and eccentricity cycles which have a well-documented calculated duration for the Quaternary ranging between 20 and 405 kyr, orbital models also predict the occurrence of million-year long cycles, corresponding to the modulations of lower order cycles (J. Laskar et al., 2011; Laskar et al., 2004). The two main longer period (>1 Myr) astronomical cycles are the g4-g3 (2.4 Myr eccentricity cycle) and s4-s3 (1.2 Myr obliquity cycle) which are in a secular resonance of 2(g4−g3) = (s4−s3) since at least 45 Ma (Jacques Laskar et al., 2011a; Laskar et al., 2004). This secular resonance however can break down to a (g4−g3) = (s4−s3) relationship where the 2.4 Myr eccentricity cycle transitions towards a 1.2 Myr cycle. A secular resonance transition has been predicted to have taken place between 50 and 100 Myr (Jacques Laskar et al., 2011a; Laskar et al., 2004). However, to date none of the published astronomical solutions for periods pre-58 Ma has shown a perfect fit with existing tuned records, when emphasis is placed on the expression of the amplitude modulation aspects of longer period (>1 Myr) astronomical cycles. Recent papers by Ma et al., (2019, 2017) indicate that a secular resonance transitions took place at ~85 Ma and ~92 Ma, but these results have not been validated by overlapping records.

The second aspect of long period (>1 Myr) astronomical imprints corresponds to the astronomical imprint on Oceanic Anoxic Event 2 (OAEII). Oceanic anoxic events (OAEs) were episodes when the extent of the oxygen poor (anoxic) waters led to extinction events and increased the burial of large amounts of organic carbon (Jenkyns, 2010, 1999; Schlanger and Jenkyns, 1976). OAEII is a minor extinction event typified by a large perturbation of the carbon cycle and the spread ocean anoxia being expressed as organic-rich black shales in the geological record (Lenniger et al., 2014; Takashima et al., 2006; Trabucho Alexandre et al., 2010). Ocean Anoxic event 2 (AOEII) occurred during the Latest Cenomanian Earliest Turonian and is the largest Ocean Anoxic event of the Cretaceous (Takashima et al., 2006; Trabucho Alexandre et al., 2010). Studies focusing on the imprint of astronomical cycles during OAEII showed an amplification of the obliquity signal in the low and middle paleolatitude records (Charbonnier et al., 2018; Kuypers et al., 2004; Meyers et al., 2012). The reason for the presence of obliquity cycles at low and middle paleolatitude during OAEII remains enigmatic. Processes such as the establishment of a high-latitude teleconnection or by an increase of the relative contribution of obliquity to astronomical-insolation have been put forwards (Meyers et al., 2012). A high latitude teleconnection

would imply that a process happening at higher latitudes where the contribution of obliquity to the insolation signal is greater can also exert a control on the processes/climate at lower latitudes. Processes with a high latitude teleconnection which can be invoked to explain the presence of an obliquity signal in low and middle paleolatitude records are: formation of high latitude intermediate/deep-water formation transporting water from the poles to lower latitudes, an obliquity modulated meridional temperature gradient impacting low-latitude wind strength or the establishment of polar icecaps changing global climate patterns (Berrocoso et al., 2008; Friedrich et al., 2008; Kuhnt et al., 1997; März et al., 2009; Nederbragt et al., 2005). Another way obliquity can influence middle to low latitudes is when obliquity controls the intensification of the monsoonal activity (Bosmans et al., 2015). The seasonal contribution of precession to insolation is opposite for both hemispheres so a seasonal increase in insolation in one hemisphere leads to a decrease in the other. As monsoonal activity is influenced by the seasonal low latitude cross-hemispheric temperature gradient the opposite influence of precession on both hemispheres effectively cancels out the contribution of precession to the monsoonal activity. Because the influence of precession on monsoonal activity is reduced changes in obliquity can therefore influence monsoonal activity to a greater degree. A high latitude teleconnection or monsoonal activity modulated by obliquity can explain the presence of an obliquity signal at middle to low latitudes, but these processes do not explain why an increase in obliquity occurred during OAEII specifically. To explain the enhanced presence of obliquity during OAEII either a relative increase of obliquity to the astronomical-insolation should have occurred during OAEII which would have amplified obliquity modulated processes in middle to low latitudes or OAEII itself changed processes in in middle to low latitudes allowing for obliquity to exert a greater on middle to low latitudes processes. To know if the contribution of obliquity to astronomical-insolation changed during OAEII longer period astronomical cycles modulating the contribution of obliquity to the astronomical-insolation need to be extracted from the record. These extracted cycles can then be used to state whether the presence of an obliquity signal during OAEII is due to an increased contribution of obliquity to astronomical-insolation or processes due to OAEII itself lead to an increased presence of obliquity.

To be able to study the behavior of longer period astronomical cycles during the late Cretaceous, a ~30 Myr long dataset covering the Cenomanian to Danian Chalk Group of the Schill Grund Platform, in the Dutch offshore is investigated. This dataset consists of petrophysical, seismic and biostratigraphic data. In this study, our aims are to integrate these datasets to investigate the presence of Milankovitch short and long cycles in the Chalk group succession on the Schill Grund Platform. Biostratigraphic data can be used to yield absolute time boundaries, allowing us to re-evaluate and identify new time constraints for stage boundaries.

The records of the Chalk Group are tuned and the 2.4 Myr eccentricity and 1.2 Myr obliquity cycles can are extracted which can then be used to check

whether the stratigraphic interval contains the secular resonance transitions (Ma et al., (2019, 2017)). Furthermore, the fit between the Chalk Group records and the expression of the amplitude modulation aspects of longer period (>1 Myr) astronomical cycles will be checked to investigate the (relative) increase in the contribution of obliquity to astronomical-insolation during OAEII.

2. Geological setting and stratigraphy

2.1 Tectonic evolution of the Schill Grund platform

The Schill Grund platform in the Dutch offshore is a structural element that is a part of the larger North Sea basin, which originated from fault trends that were formed during the Caledonian orogen (figure 1) (De Jager, 2007; De Vos et al., 2010; M. C. Geluk, 2007; Pharaoh et al., 2003). These faults trends were later reactivated three times, during the late Carboniferous Variscan orogeny, the Permian orogenic collapse, the early Triassic to early Cretaceous failed rift phase and late Cretaceous to Paleogene inversion events (Bachmann et al., 2010; M. M. C. Geluk, 2007; Kombrink et al., 2010; van Buggenum and Den Hartog Jager, 2007; Vejbæk et al., 2010; Wong et al., 2010). During the Jurassic a failed rift phase started which induced salt movements in the Permian salts present at the Schill Grund Platform into salt pillows (Ten Veen et al., 2012). During the early Cretaceous, rifting halted and a post-rift thermal sag phase started. The combination of a thermal sag phase and a global eustatic sea-level rise led to an overstepping of the basin margin (Herngreen and Wong, 2007; Van der Molen, 2004; Vejbæk et al., 2010). The early Cretaceous rise in sea-level led to a progressively decreasing continental influence and initiated the transition from the Lower Cretaceous argillaceous claystone dominated Lower Rijnland Group to the open marine carbonate facies of the Upper Cretaceous Chalk Group (Herngreen and Wong, 2007)

During the late Cretaceous the alpine orogeny manifested itself in the Dutch offshore as multiple inversion phases related to the Subhercynian and Laramide tectonic events, which led to inversion in the basins in the Dutch offshore while deposition continued on the platforms and structural highs (figures 1 and 2) (Herngreen and Wong, 2007; Van der Molen, 2004; Vejbæk et al., 2010). The deposition of the Chalk Group was heavily influenced by the Subhercynian and Laramide tectonic events, which reduced the stratigraphic completeness of the basins adjacent to the Schill Grund platform. The Northern Dutch offshore was impacted by a south west tilting during the Turonian and continuous subsidence took place in the eastern Dutch offshore during the Coniacian to Santonian (Van der Molen, 2004; Van der Voet, 2015). Two inversion pulses occurred in the Campanian to Maastrichtian in the Dutch Northern offshore (Van der Voet, 2015). The Step Graben, western Dutch Central Graben and Terschelling basin were inverted during the first pulse and the Elbow Spit Platform was inverted during the second pulse. The inversion in combination with the inherent instability of the chalk sediments led to erosion and redeposition, which manifested itself as

slumps, slides, channels and frontal splays. The inversion phases also led to a renewed phase of salt movement in the Dutch offshore which heavily impacted the structural basins in the Dutch Offshore, but barely impacted the Schill Grund Platform (Ten Veen et al., 2012). The Laramide tectonic phase occurred during the latest Cretaceous/early Paleogene and initiated a shift from a carbonate to siliciclastic dominated depositional environment and ending the deposition of chalk in the Dutch offshore (Knox et al., 2008; Wong et al., 2007). Considering that the Schill Grund platform remained undeformed, it is therefore the ideal location to conduct a cyclostratigraphic study on the Chalk Group.

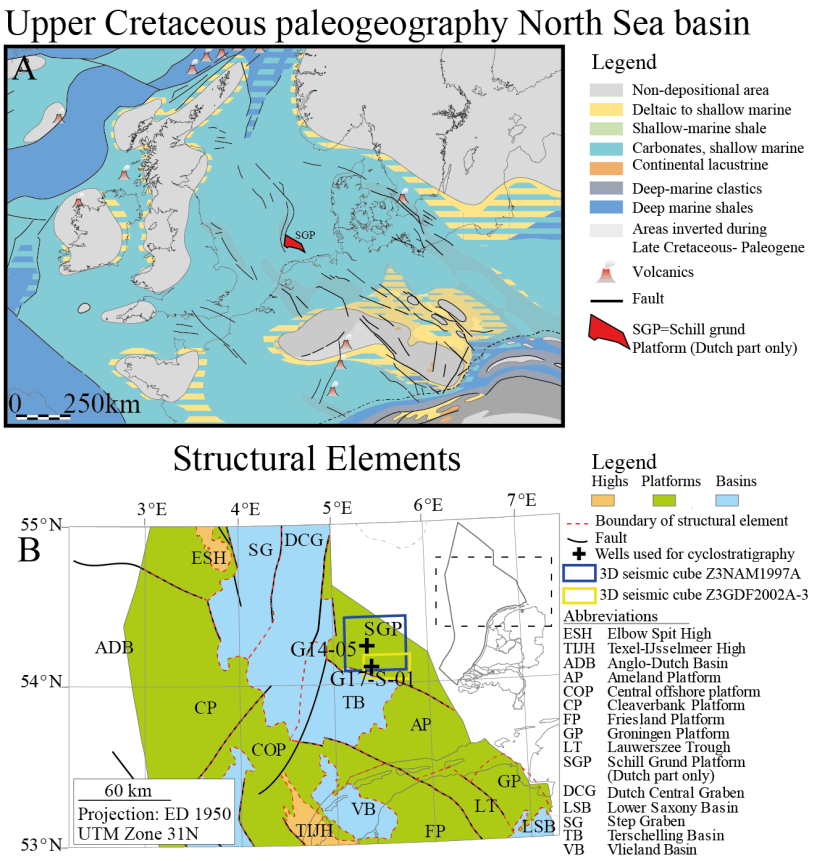

Figure 1. A: Upper Cretaceous paleogeography of the North Sea basin and adjacent areas, modified after O.V. Vejbæk et al.(2010). Indicated by the red box is the paleo-location of the Schill Grund platform. B: structural elements in the Dutch offshore, modified after Kombrink et al.(2012). Indicated on the map are wells G14-05 and G17-S-01, which are the wells being investigated for an imprint of astronomical cycles.

2.2. Chalk Group Stratigraphy

The Chalk Group in the Dutch offshore is divided into 3 stratigraphic units: the Texel, the Ommelanden and the Ekofisk Formations (van Adrichem Boogaert and Kouwe, 1994; Van der Molen, 2004) (Figure 2). The Texel Formation, of Cenomanian age consists of white to beige marly chalks and limestones. The top of the Texel Formation is defined by the Plenus Marl Member, made of dark-grey to locally black calcareous bituminous claystones and marls. The Plenus Marl Member -is up to 10 meters thick and coincides with OAEII (Niebuhr et al., 2001; Schlanger et al., 1987). In well G17-S-01 the Plenus Marl can be divided upper and lower Plenus marl/shale beds, identified by two large peaks in the Th record, two smaller peaks in the sonic log and a decrease in the density log (Van der Molen, 2004).The upper and lower Plenus marl/shale beds have been linked to two known phases of expanding anoxia and increasing ^{13}C values (Clarkson et al., 2018; Danzelle et al., 2018; Laurin et al., 2016).

The Ommelanden Formation consists of an alternation between white to beige chalks and more clay rich light-olive-green to grey chalks. The chalk is generally fine-grained. Flint nodules are common within this Formation. The top of the Ommelanden Formation is of Latest Maastrichtian to early Danian age and is defined by a large shift towards higher GR and sonic values.

The Ekofisk Formation is of Danian age and consists of an alternation of white chalks and grey/green clay rick laminated chalks (van Adrichem Boogaert and Kouwe, 1994; Van der Molen, 2004). Nodular and bedded flint layers and glauconite rich beds are also present. The Ekofisk Formation is characterized by resedimented facies and by high amplitude seismic reflectors.

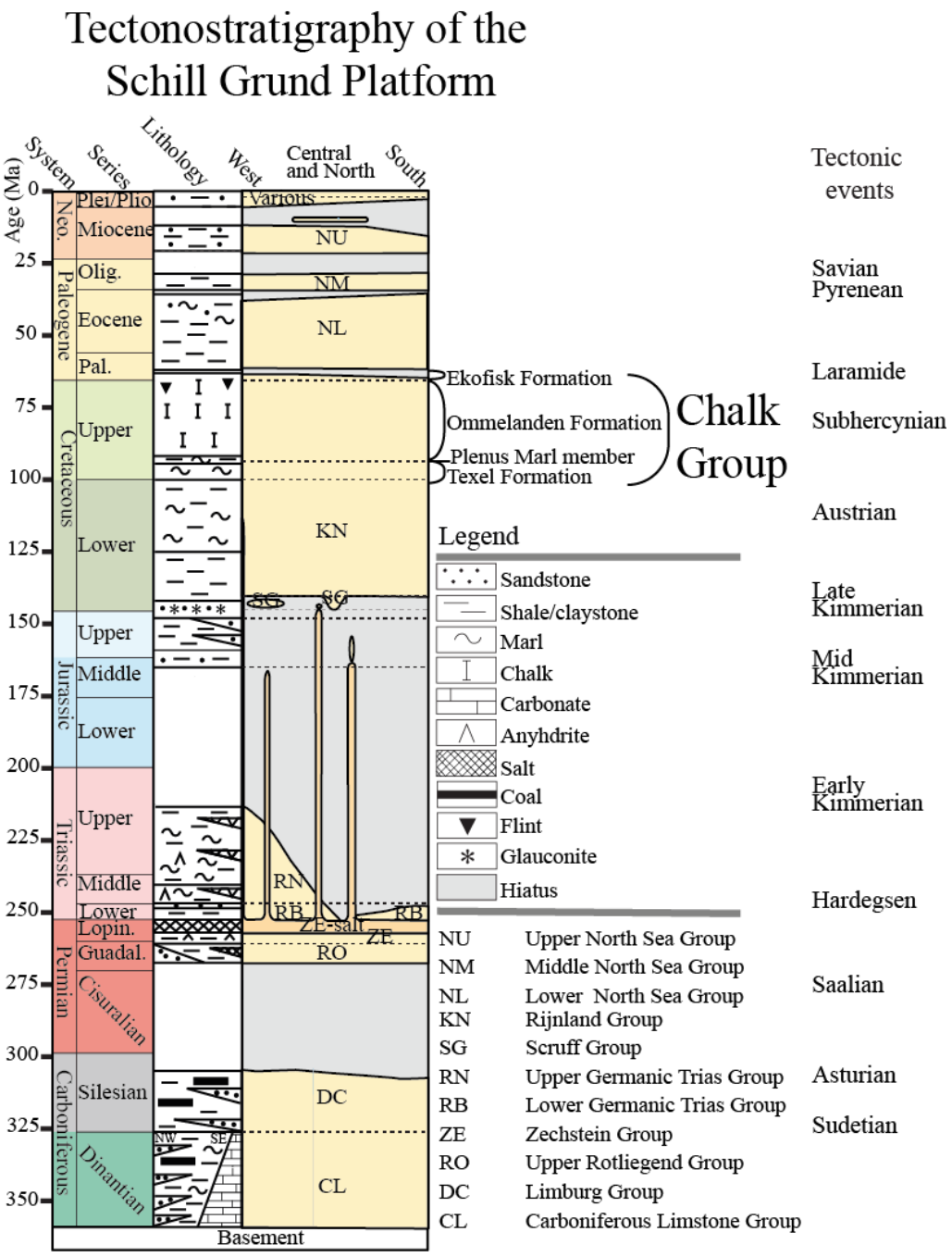

Figure 2.Tectonostratigraphy of the Schill Grund Platform, modified after TNO (2011).

3 Material and methods

3.1 Dataset

The dataset used in this study consists of seven 3D seismic surveys, two 2D seismic surveys, 15 wells, mapped surfaces and a velocity/depth model. These data were provided by TNO-GDN. Detailed descriptions of the used data and the data itself can be freely accessed via https://www.nlog.nl/datacenter/. The exact locations of the seismic and well data can be found in SI Figures S1 and S2 10.1 and 10.2. The 3D seismic covers most of the Dutch part of the Schill Grund Platform and adjacent parts of the Dutch Central Graben, Terschelling Basin and Ameland Platform. The seismic lines from 2D surveys Z2NOP1987A-6 and Z2NOP1983A2D cover most of the northern and central part of the Dutch Offshore sector and are used as a regional correlation tool between the different 3D seismic surveys. All the used wells penetrate the Chalk Group. The data from the wells consists of Meta data (identification information, location, drilling purpose and results, client information and current operational status) and a geological/geophysical dataset (vertical seismic profiles (VSP's), checkshots, well-logs, or cuttings-based calcareous nannofossil biostratigraphy, lithologs, drillings reports and deviation data). The Group based layers from TNO-GDN's DGM-diep V5 offshore dataset are used for a first order correlation between the seismic and well-log datasets. TNO-GDN's Velod-3.1 velocity model is used for the time-depth conversion of the seismic data.

The key wells used to investigate the presence of astronomical cycles are wells G14-05 and G17-S-01 (Figure 3). The other investigated wells are used for correlation purposes, to calculate sedimentation rates based on calcareous nannofossil biostratigraphy and to use the biostratigraphy to constrain the K/Pg boundary to a specific seismic reflector. Well-logs are measured using well-logging tools, which do not do direct spot measurements, but measure the properties within a certain interval a so-called cone of influence. Because of this complication, high frequency changes within well log are smoothed out and are therefore not detectable. To assess the resolution of well-logs and thus the minimum detectable cycle length, one can use the log association parameter (LAP) which calculates the minimum period (meters) detection limit for cycles in different well-logs (Worthington, 1990). The minimum detectable cycle lengths according to the LAP is 1.2 m for (spectral) GR logs (Worthington, 1990).

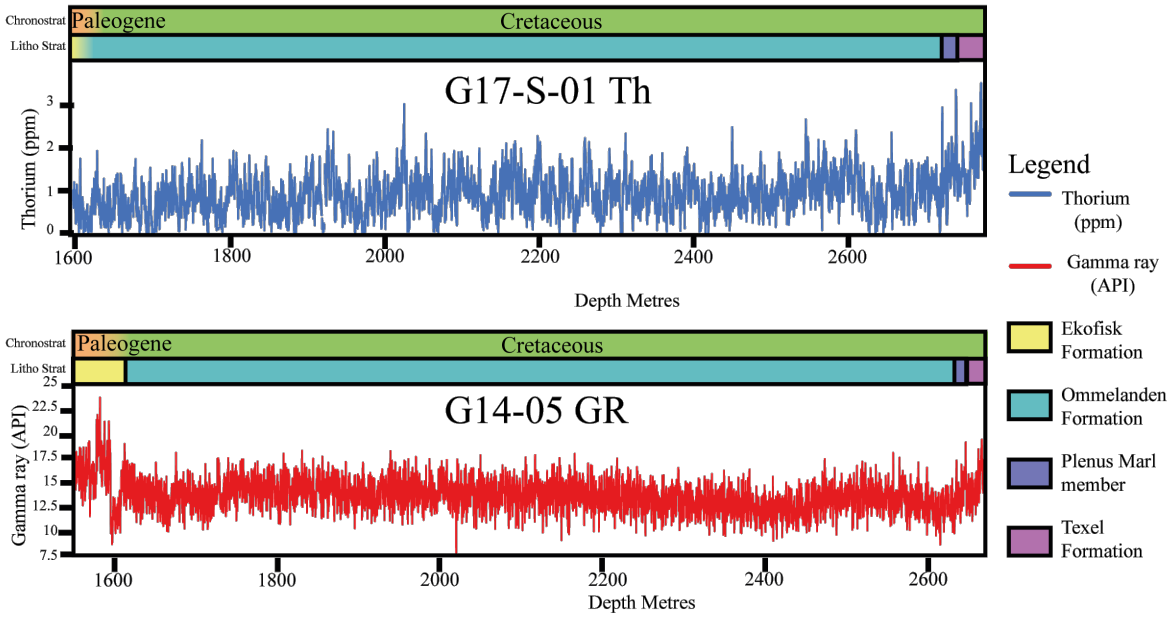

Figure 3. Top window Thorium log G17-S-01 with chronostratigraphy and lithostratigraphy. Bottom window Gamma ray log G14-05 with chronostratigraphy and lithostratigraphy. Lithostratigraphy and chronostratigraphy based on (TNO-GDN, 2022).

3.3 Software and analytical tools

To investigate the presence of astronomical cycles we used two software programs. The first program is Petrel, which is an integrated geoscientific interpretation software used to handle the seismic and well-log data input types (Schlumberger). The seismic data, well-logs and the Group based layers from TNO-GDN's DGM-diep V5 offshore dataset are plotted in Petrel to check if the top and bottom of the Chalk Group are correctly placed in both the seismic and well-log data. This check is done to avoid any erroneous correlations. The well-log data is then exported from Petrel and imported into the software platform R (R Core Team, 2020) in which the Astrochron (Meyers, 2014) and Biwavelet (C. Gouhier et al., 2019) packages are used to identify astronomical cycles, to create age models and to filter the cycles from the well-logs. Wavelet analysis and Evolutive Harmonic analysis (EHA, Astrochron) are applied to the well-logs to identify the stratigraphic evolution of (astronomical) cycles in the Chalk Group (C. Gouhier et al., 2019; Meyers, 2014). The wavelet spectral analysis (Biwavelet) is used as the main tool to identify the different period cycles. The major advantage of a continuous wavelet transform is that the smallest to the largest length cycle frequency/period can be analyzed and visualized in one

figure. The EHA is a windowed multi-taper method (MTM) harmonic analysis used to infer spatial changes in the dominant frequency in stratigraphic sections, by creating a spectrum for each of the windowed studied intervals (Thomson, 1982). The MTM harmonic analysis can provide a statistical significance (F-variance ratio test) for each frequency component which allows one to quantify the statistical significance of spectral peaks. Evolutive Average Spectral Misfit (eASM, Astrochron) uses the previously created EHA spectra and compares the ratio between the spectral in the EHA spectra to a set of astronomical cycles to compute the statistically most likely sedimentation rate(s) (Meyers, 2012; Meyers et al., 2012; Meyers and Sageman, 2007). The resulting figure indicates the sedimentations rates in the depth domain with a statistical confidence level.

The EHA spectra, wavelet spectra and eASM derived sedimentation rates are compared with (bio) stratigraphic age constraints. Together these results enable us to interpret astronomical cycles in the well-logs. An EHA spectra is used to track the frequency of the 405 kyr eccentricity cycle which enables to track and make sedimentation rates curves for wells G14-05 and G17-S-01. These sedimentation rate curves are then used to convert the well-logs from the depth domain to the time domain. The (bio) stratigraphic age tie-points are used to tie in the well-logs to the correct geological age.

The 405 kyr cycle is filtered from orbital solution la2010d and subsequently aligned to the 405 kyr cycles filtered from the records form wells G14-05 and G17-S-01 in the time domain.

Using the two techniques described in Ma et al. (2017) the amplitude modulation of eccentricity and obliquity is extracted from the well-logs (in the time domain) as well as from astronomical solutions la2004, La2010a-d 2011, ZB17a-p and ZB18, allowing us to see how amplitude modulating cycles behave during the late cretaceous especially with respect to the chaotic resonance observed in Ma et al., (2019, 2017) and the how amplitude modulating cycles modulate the expression of obliquity during OAEII. The two techniques described in Ma et al. (2017) which extract amplitude modulating cycles from (proxy)records is preferred over filtering out cycles because the two techniques of Ma et al. (2017) avoid the pitfall that when one filters out a specific period/bandwidth from a record one filters out all cycles within set specific period/bandwidth and not a specific astronomical cycle. The studied records contains and interval which according to Ma et al., (2019, 2017) that contains a secular resonance transitions in which the 2.4 Myr eccentricity cycle transitions to a cycle with a 1.2 Myr duration and then back to a duration of 2.4 Myr. A filter cannot distinguish between two cycles which originate from different astronomical parameters but have the same period, so in this case filtering out the 1.2 Myr obliquity cycle will also filter out 1.2Myr eccentricity during a chaotic resonance transition. The technique of Ma et al. (2017) avoid this issue by separately extracting amplitude modulation records of the eccentricity and the obliquity before the 2.4 Myr eccentricity and 1.2 Myr obliquity cycles are filtered out from the record. The first technique of (Ma et al., 2017) extracts the spectral power of eccentricity

and obliquity from an EHA in spectra in the time domain. Spectral power is modulated by higher order cycles which in this case allows one to distinguish between a 1.2 Myr Obliquity cycle modulating obliquity spectral power and a 2.4 Myr eccentricity cycle transitioning towards a 1.2 Myr cycle during a chaotic resonance transition modulating the spectral power of eccentricity. In this study the spectral power and of the 405 kyr eccentricity and 173kyr obliquity cycles are extracted from an EHA spectra. The second technique of Ma et al. (2017) extracts extract the amplitude modulation by performing a Hilbert transform on filtered records of lower order astronomical cycles. In this study the 405 kyr ecc and 173 kyr cycle obliquity cycles are filtered from the tuned record. On these filtered records a Hilbert transform is conducted after which 2.4 Myr eccentricity and 1.2 Myr obliquity cycles can be filtered. Using the extracted spectral power and amplitude modulation results, it is possible to study the behavior 2.4 Myr eccentricity and 1.2Myr obliquity cycles separately helping us to verify the previously identified chaotic resonance in Ma et al. (2019, 2017) and to check whether any of the current astronomical solutions accurately models the amplitude modulation of the 2.4 Myr eccentricity and 1.2 Myr obliquity prior during and after the chaotic resonance transition identified Ma et al. (2019, 2017). The extracted 2.4 Myr eccentricity and 1.2Myr obliquity cycles can also be used to quantify the contribution of obliquity and eccentricity to astronomical-insolation during OAEII, which might help explain the enigmatic presence of obliquity during the latter part of OAEII.

4. Results

To investigate the presence of astronomical cycles, we focus on the Gamma ray (GR) of Well G14-05, and on the Thorium (Th) log of well G17-S-01. Both GR and Th logs have successfully been used in cyclostratigraphic stratigraphic studies in the past (Ten Veen and Postma, 1996; Wu et al., 2014, 2013). The sedimentological and stratigraphic relevance of Th and GR is useful for defining a phase relation between the astronomical cycles and the sedimentology. According to Ellis and Singer, 2007, Th record is a proxy for detrital input, while the GR signal from well-log G14-05 is the cumulative value of the radioactive elements Potassium, Thorium and Uranium. The combination of these elemental abundances allows us to estimate the shale content of the sediments (Ellis and Singer, 2007). Well G14-05 has no separate Th log available and thus only the gamma-ray log will be used to investigate the presence of cycles. The complex composite environmental signal of the GR log hinders a straightforward interpretation, however well G17-S-01 indicates that the bulk of the GR signal in the Chalk Group is from the element's potassium, and thorium, while uranium is only a minor contributor to the GR signal. Since potassium and Thorium both are proxies for the detrital/clay fraction (Ellis and Singer, 2007), one can assume that the GR signal in well G14-05 is an indicator of the detrital fraction. This assumption allows us to use both GR and Th as proxies for detrital input in wells G14-05 and G17-S-01. Due to the composite environmental nature of

the Gamma-ray log, the results of G14-05 are however to be expected of lower quality than those of G17-S-01.

4.1 Spectral analysis

4.1.1 Wavelet and MTM analysis

The wavelet and MTM results reveal that spectral power is concentrated in frequency bands that correspond to the periods of ~4-6, ~8-12, ~12-25, ~32, ~40-60, ~80-120 and ~150-250 m (Figure 4). In the wavelet spectra the observed cycles do not have a stable period nor a stable spectral power, which is due to changes in sedimentation rate and the modulating effect of higher order astronomical cycles.

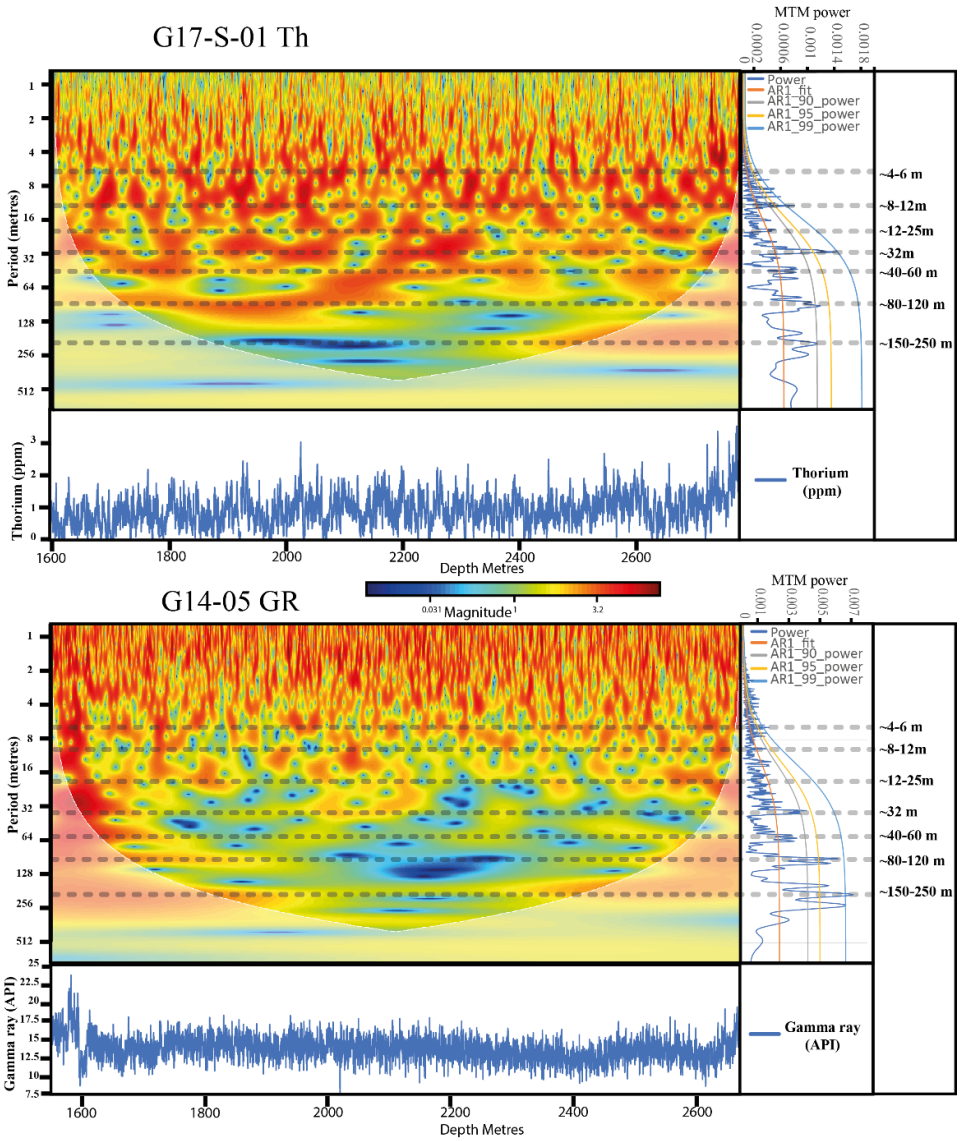

Figure 4. Wavelet spectra in the depth domain of well-logs G14-05 Gr and G17-S-01. To the right of the wavelet figures are the MTM spectra of the well-logs. Indicated in the grey dotted lines are cycles/periods with high spectral power.

4.1.2 eASM

The 2.4, 1.6 and 1.2 Myr, 966, 812, 688, 405, 200, 173 and 110 kyr astronomical cycles (Hilgen et al., 2020; Hinnov, 2000; Laskar et al., 2004) were used as target orbital frequencies for the eASM analysis on the EHA spectra of well-logs G14-05 Gr and G17-S-01 Th. The 95, 97, 99, 105, 124 and 131 short eccentricity cycles were combined into a single 110 kyr term as these cycles have such a close temporal spacing that distinguishing between these cycles in a spectrum is impossible. The eASM analysis is set up to go through sedimentation rates ranging between 1 and 25cm/kyr, which covers the spectrum of sedimentation rates stated in current literature for the Chalk Group of the Southern Permian Basin (Boussaha et al., 2016; Damholt and Surlyk, 2004; Niebuhr et al., 2001; Niebuhr and Prokoph, 1997; Pearce et al., 2020; Perdiou et al., 2015; Van der Molen, 2004; Voigt and Schönfeld, 2010; Zijlstra, 1994). The EHA spectra on which the eASM analysis was conducted has a 200 m sliding window and frequency range of 0.005-0.5 cycle/meter. The eASM results show the statistically most likely sedimentation rates (e.g. brightest color) ranging between 3 to 7.5 cm/kyr (see figure 5). The eASM results of G14-05 GR are of lower quality than those of G17-S-01 Th which is as expected, because the GR log is of lesser quality when compared to the Th log (see chapter 3.1).

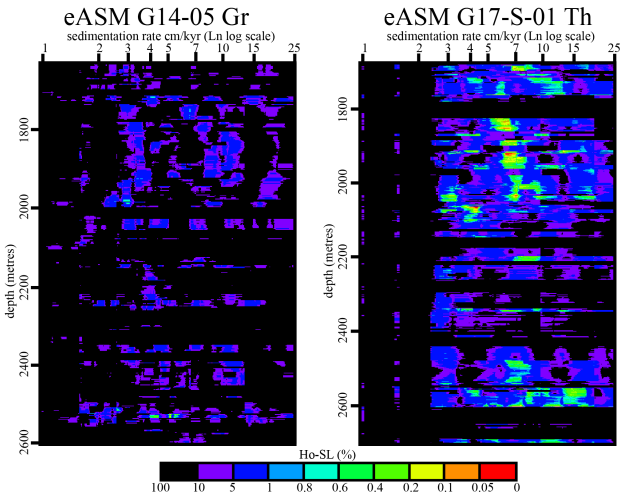

Figure 5. eASM results right: eASM plot G17-S-01 Th log. Left: eASM plot G14-05 Gr. Ho-Sl (%) is null hypothesis. A lower null hypothesis indicates a better statistical fit between input cycles and the EHA spectra at a given sedimentation rate.

4.2 Sedimentation rate estimates and cyclostratigraphic interpretations

To check the validity of the sedimentation rates obtained through eASM we investigated the (bio)stratigraphy of the Chalk Group. The existing well cuttings-based calcareous nannofossil biostratigraphy of the Chalk Group in the Dutch Offshore was compiled and assigned ages which enabled the identification of stage boundaries which were then be used as tie-points and to calculate the average sedimentation rate between these stage boundaries (see SI Table S1).

For wells where the K/Pg boundary could be identified based on the biostratigraphy, a specific seismic reflector could be identified for the K/Pg boundary for the Schill Grund Platform and adjacent areas. In the seismic data with a

Zero phase North Sea polarity the S-wave crossing above the third peak below the top of the Chalk Group was identified as the reflector which coincides with the K/Pg boundary. In the Petrel standard seismic color scheme with Zero phase North Sea polarity that means that the white reflector above the third red reflector indicating the top of the Chalk group coincides with the K/Pg boundary (see SI Text S1 and Figure S3 for a more in-depth explanation using well G16-02).

The cuttings-based calcareous nannofossil biostratigraphy enabled the identification of stage boundaries which enabled us to calculate the average sedimentation for these stages. Wells G17-01 and F15-01 have the best biostratigraphic age constraints, and both indicate sedimentation rates around ~4 cm/kyr for the Chalk Group (see SI Table 1), which is similar to the eASM results (3.0-7.5 cm/kyr see chapter 4.1.2).

The sedimentation rates derived from biostratigraphy and, eASM allows us to assign the spectral peaks found in the wavelet and MTM spectral analysis to astronomical cycles thus identifying the 4-6 m cycles as the 100 kyr short eccentricity cycle, the 8-12 m cycles as the 173-183 kyr obliquity cycle, the 12-25 m cycle as the 405 kyr eccentricity cycle, the 32 m cycle as the 800 kyr eccentricity cycle, the 40-60 m cycle as the 1.2 Myr obliquity cycle, the 80-120 m cycles as 2.4 Myr eccentricity and the 150-250 m cycle as the 4.6 Myr eccentricity cycle.

4.3 Depth time conversion

The duration of the 405 kyr eccentricity cycle is the most stable cycle during the Cretaceous and will therefore be used to convert the records from the depth domain to the time domain (Laskar, 2010). An EHA spectra (100 m window, frequency range of 0.01 to 0.1 cycles per meter) tracks the 405 kyr cycle in the depth domain and gives us a sedimentation rate curve which is then used to convert the data from the depth to the time domain (see Figure 6A & 6B).

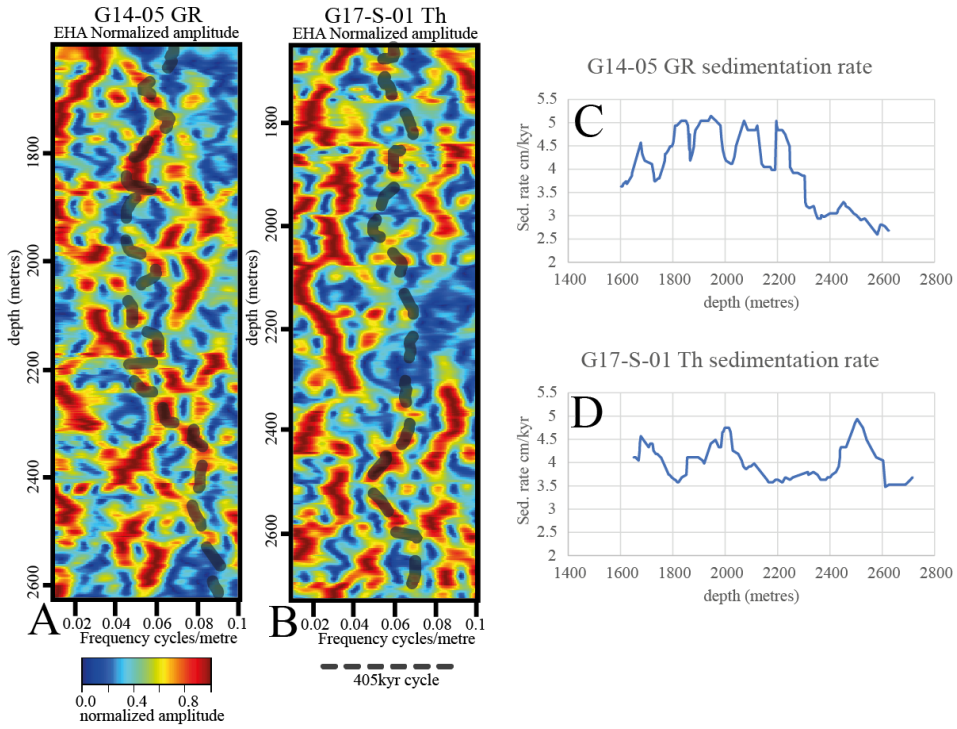

Figure 6. A. EHA spectra of G14-05 Gr with the 405 kyr eccentricity cycle traced in grey B. EHA spectra of G17-S-01 Th with the 405 kyr eccentricity cycle traced in grey. C. Sedimentation rate curve extracted from the traced 405 kyr eccentricity cycle in the EHA spectra of G14-05 GR. D. Sedimentation rate curve extracted from the traced 405 kyr eccentricity cycle in the EHA spectra of G17-S-01 Th.

4.4. Cyclostratigraphic framework

4.4.1 Proxy record and its astronomical phase relationship

Usually comparing the Hilbert transform of the precession, obliquity or short eccentricity to the spectral filtering of respectively short eccentricity, 173 kyr obliquity and long eccentricity allows one to infer the phase of a proxy with respect to the insolation curve. In this study, precession and obliquity are below or near the detection limit, while the 100 kyr eccentricity cycle has low spectral power and an overall noisy signal component, which makes it impossible to use Hilbert transform of these cycles to infer a phase relationship. A phase relationship based on existing literature and basinal setting is inferred instead in which the highest values of the detrital proxies (GR and Th) correspond to eccentricity maxima. This phase relationship could be explained that seasonal contrast

increases during eccentricity maxima, leading to a stronger summer monsoonal activity with increased precipitation, weathering rates and runoff leading to an enrichment in detrital proxies (Ruddiman, 2008; Ten Veen and Postma, 1996; Wu et al., 2014, 2013). An anti-phase relationship between Milankovitch cycles and detrital proxies is also possible, through the eccentricity minima modulated stagnation, leading to the formation of anoxic bottom waters and to a relative enrichment in detrital proxies (Herbert and Fischer, 1986; Liebrand et al., 2018). The fact that the chalk group contains a large submarine channel system stretching from Norway offshore sector all the way into the Dutch offshore, indicates a dynamic environment with large moving water masses hindering basinal stagnation and therefore an in-phase relationship between Milankovitch cycle and detrital inputs in inferred (Esmerode et al., 2008, 2007; Esmerode and Surlyk, 2009; Gennaro and Wonham, 2014; Hampton et al., 2007; Jarvis, 1980; Lykke-Andersen and Surlyk, 2004; Remin et al., 2016; Surlyk et al., 2008; Surlyk and Lykke-Andersen, 2007; Van der Molen, 2004)..

4.4.2 Age tie point and tuning to La2010d

To turn the floating age to one with absolute ages, the record is anchored to the K/Pg boundary subsequently tuned to La2010d. The record is specifically tuned to La2010d because the 405 kyr eccentricity cycle filtered from this solution has been proven to be a good fit for tuning late Cretaceous geological records (Ma et al., 2017; Wu et al., 2014). Furthermore, La2010d is also favored over La2010a, La2010b and La2010c as it is adjusted to INPOP06 over the last 1 Myr and includes the five major asteroids, Ceres, Vesta, Pallas, Iris, and Bamberga, which makes it the most constrained version in the La2010 models (Jacques Laskar et al., 2011a, 2011b; Westerhold et al., 2012). To anchor the record to the K/Pg boundary the available biostratigraphy was used to constrain the K/Pg to a single seismic reflector which could then be traced into wells G17-S-01 and G14-05 giving and approximate location of the K/Pg boundary in the well-logs (see SI Figure S4). The phase relationship between the 405 kyr eccentricity cycle and the K/Pg boundary is already known as being just past a minimum in the 405 kyr cycle (Batenburg, 2013; Batenburg et al., 2014, 2012; Friedrich et al., 2016; Husson et al., 2011; Westerhold et al., 2008). By combining the 405 kyr cycle filtered from the well-logs in the time domain, the known 405 kyr eccentricity cycle to K/Pg boundary and the biostratigraphy and seismic based location of K/Pg boundary in the well-log based, it was possible to constrain the K/Pg boundary to a specific 405 Kyr cycle filtered from the well-logs allowing us to anchor the floating timescale of the well-logs to K/Pg boundary. With the record anchored to the K/Pg boundary it is possible to (re)tune the record to la2010d, through fitting 405 kyr maxima fitting in the records to the eccentricity maxima in la2010d (figure 7) (for a comparison between a record solely anchored to the K/Pg boundary and one to La2010d see SI Figure S5, S6 and S7). By having the records with absolute ages it allows us to now to check whether the chaotic resonance transition observed by Ma et al., (2019, 2017) is also present in our records.

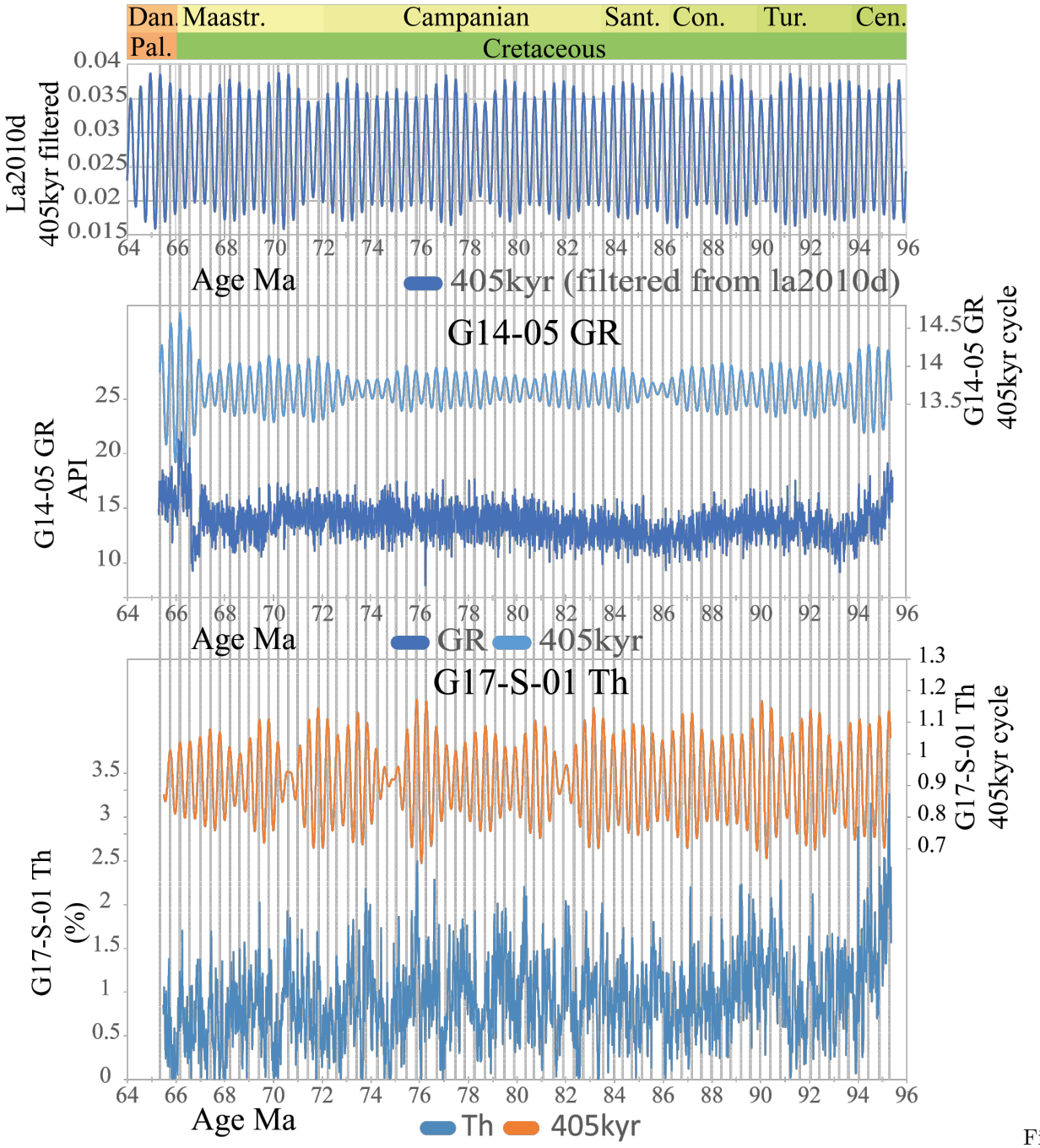

7. Well-logs G14-05 GR and G17-S-01 Th tuned to La2010d. The grey lines indicate the 450kyr eccentricity maxima from filtered la2010d. Above the tuned records of G14-05 GR and G17-S-01 Th tuned is the 405 kyr eccentricity

cycle filtered from set records.

4.4.5 Spectral analysis in the time domain

A wavelet and MTM spectral analysis were performed on the well-logs after tuning to La2010d. The wavelet spectra (Figure 8) shows that the Th record of G17-S-01 has significantly more spectral power concentrated at known periods of astronomical cycles when compared to the GR record of G14-05. A difference in the quality of results was already observed in the spectral analysis in the depth domain and the eASM results (figure 4 and 5) of wells G17-S-01 Th and G14-05 Gr. The quality of results is as expected because of the composite environmental nature of the Gamma-ray log of G14-05 when compared to the Th log G17-S-01. The wavelet and MTM spectral analysis (Figure 8) of both G14-05 and G17-S-01 show high spectral power for the known 173, 200, 405, 688, 812 and 977 kyr and 1.2, 1.6, 2.4 and 4.7 Myr astronomical cycles. The short eccentricity cycles have a relatively high noise component overprinting the original signal. Both obliquity and precession cannot be distinguished from the spectral noise. Due to fact that we tuned the records to the 405 kyr cycle we do see that the 405 kyr cycle is the cycle with the highest statistical significance and most the prominently defined spectral peak.

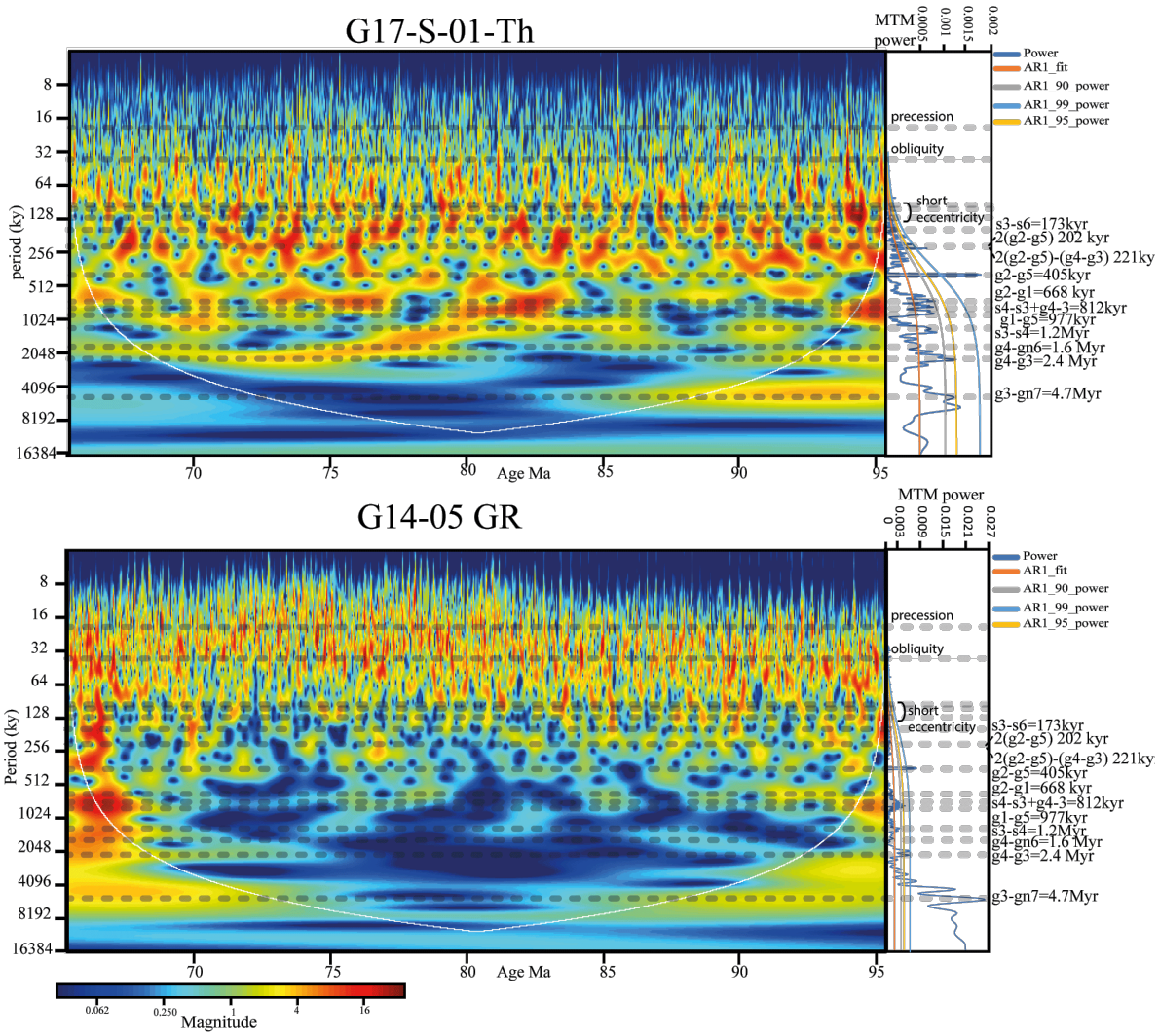

Figure 8. Wavelet spectra of well-logs G14-05 GR and G17-S-01 Th tuned to La2010d. The black dotted lines are periods of know astronomical cycles. To the right of the wavelet spectra are the MTM spectra applied to the whole interval. To the right of the MTM spectra are the fundamental frequency combinations and durations for the identified astronomical cycles. The white line in the wavelet spectra is the 95% confidence interval

4.5 Amplitude modulation and comparison with different orbital solutions

The Thorium record of G17-S-01 is the main record to study the amplitude modulation because of the complex and more noisy nature of the Gamma-ray record of G14-05 makes it less suitable to study the amplitude modulation. Using the two techniques described in Ma et al. (2017) the amplitude modulation of eccentricity and obliquity was extracted from the well-logs (in the time domain) as well as from astronomical solutions la2004, La2010a-d 2011, ZB17a-p and ZB18 (figure 9 and SI Figure S8). For the methodology and how the techniques described in Ma et al. (2017) were implemented see chapter 3.3. The resulting amplitude modulating records make it is possible to directly check if the secular resonance transitions observed in Ma et al., (2019, 2017) is present in the records of the Chalk Group and if any of the amplitude modulation records of astronomical solutions accurately model these secular resonance transitions. The Amplitude modulation in combination with filtered record 405 kyr ecc and 173 kyr cycle also allows us to assess the contribution of obliquity to astronomical-insolation during OAEII which can help us the enigmatic presence of an obliquity signal during the latter part of OAEII.

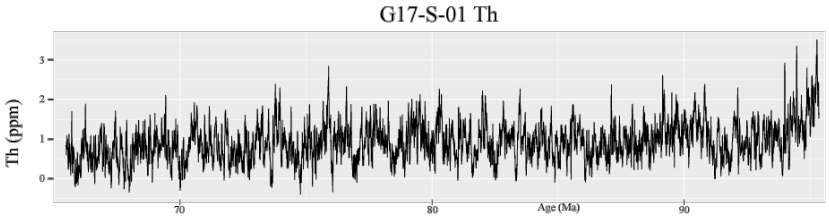
G17-S-01 Th
Th (ppm)
Age (Ma)

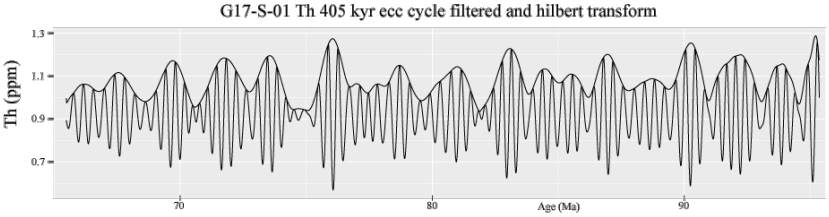
G17-S-01 Th 405 kyr ecc cycle filtered and hilbert transform
Th (ppm)
Age (Ma)

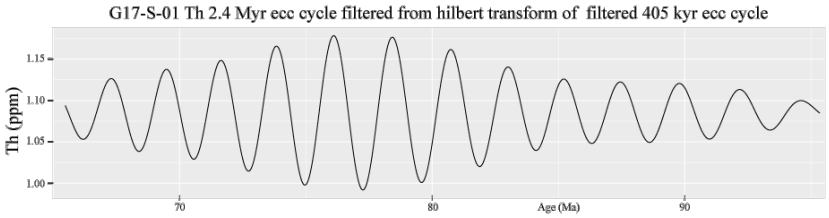
G17-S-01 Th 2.4 Myr ecc cycle filtered from hilbert transform of filtered 405 kyr ecc cycle
Th (ppm)
Age (Ma)

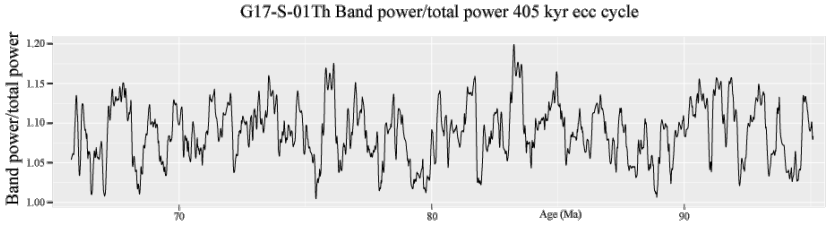
G17-S-01Th Band power/total power 405 kyr ecc cycle
Band power/total power
Age (Ma)

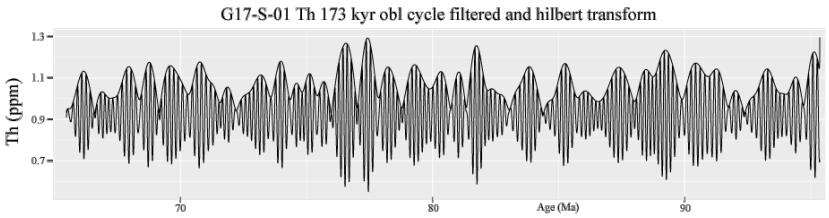
G17-S-01 Th 173 kyr obl cycle filtered and hilbert transform
Th (ppm)
Age (Ma)

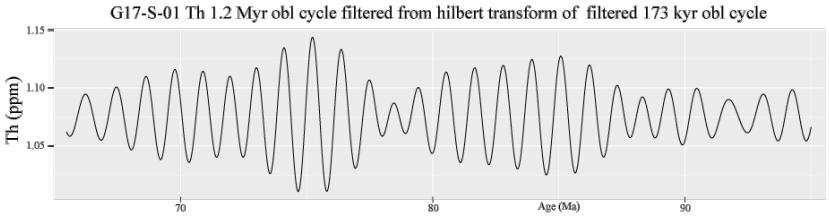
G17-S-01 Th 1.2 Myr obl cycle filtered from hilbert transform of filtered 173 kyr obl cycle
Th (ppm)
Age (Ma)

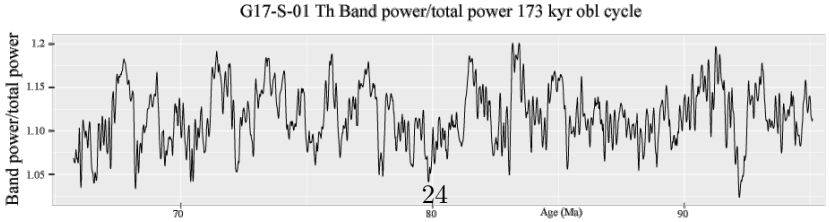
G17-S-01 Th Band power/total power 173 kyr obl cycle
Band power/total power
Age (Ma)

Figure 9. Filtering and amplitude modulation extracted from G17-S-01 Th

5. Discussion

5.1 Late Cretaceous secular resonance transition

Currently the 2.4 Myr eccentricity and 1.2 Myr obliquity cycles are in a 2:1 secular resonance state expressed as the 2(g4−g3)=(s4−s3) principal frequency terms (Jacques Laskar et al., 2011a; Laskar, 1999; Laskar et al., 2004). This secular resonance relationship can break down to (g4−g3) = (s4−s3) causing the 2.4 Myr eccentricity cycle to change to a cycle with a 1.2 Myr cycle period, which has been predicted to have been occurred between 50 and 100 Myr (Laskar et al., 2004). The duration of the 2.4 Myr eccentricity cycle itself can also change due to chaotic diffusion by the gravitational interactions of the Solar System which has been observed in the records from the Triassic-Jurassic Newark-Hartford basin in which that the period of the of the 2.4 Myr eccentricity decreased to a 1.75 Myr period (Olsen et al.,2019). Studies by Ma et al., (2019, 2017) have shown that a secular resonance transition took place at ~85 Ma and at ~92 Ma. During the ~92 Ma resonance transition the duration of the 2.4 Myr long eccentricity cycle decreased to 1.2 Myr, while during the ~85 Ma resonance transition the 1.2 Myr long eccentricity cycle had its period restored back to a 2.4 Myr period. A secular resonance transition impacting the 2.4 Myr eccentricity cycle is also observed in this study. Around ~92 Ma the 2.4 Myr eccentricity cycle reduces in amplitude and period and only fully reverts back to a 2.4 Myr duration at ~85 Ma (Figure 10). Outside the period impacted by the secular resonance transition the duration of the 2.4 Myr eccentricity remains stable indicating that the duration of the 2.4 Myr eccentricity was not impacted by chaotic diffusion in the gravitational interactions of the Solar System as is the case for the Triassic-Jurassic Newark-Hartford basin (Olsen et al.,2019). To check if any of the existing astronomical solutions accurately models the amplitude modulation of the 1.2 Myr obliquity and 2.4 cycles extracted from the tuned well-log Myr before during and after the chaotic resonance the modulation extracted from the tuned well-log records were compared with the modulation extracted from astronomical solutions (see SI Figures S9 and S10). None of the eccentricity or obliquity amplitude modulation records extracted from astronomical solutions fits with the amplitude modulation extracted from the well-logs. This indicates that none of the current astronomical solutions accurately models the late cretaceous chaotic resonance transitions observed in this study and Ma et al., (2019, 2017), indicating the need for new astronomical solutions, which do accurately model the Late Cretaceous chaotic resonance transitions.

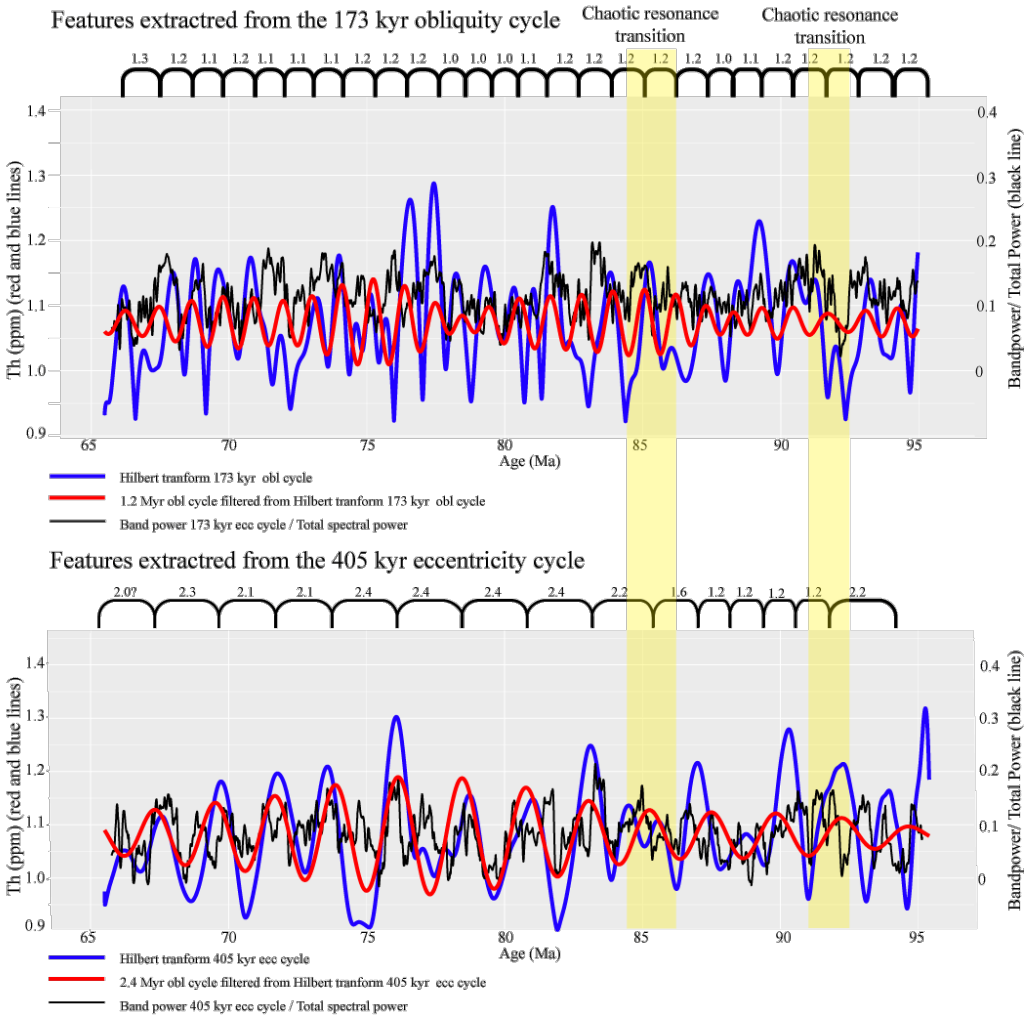

Figure 10. Astronomical features of the 1.2Myr obl and 2.4 Myr ecc extraction from G17-S-01 Th in the time domain. Astronomical features that are shown are the band power of the 405 kyr ecc and 173 kyr obl cycle divided by the total spectral power (black line), The Hilbert transformed signal from the filtered 173 kyr obl and 405kyr ecc cycles (blue lines), the 1.2 Myr obl cycle filtered from the he Hilbert transformed signal from the filtered 173 kyr obl cycle and the 2.4 Myr ecc cycle filtered from the he Hilbert transformed signal from the filtered 405 kyr ecc cycle (red lines). The yellow bars indicate the two periods when a secular resonance transition took place. The chaotic resonance transition can be observed by the mismatch between the 2.4 Myr cycle filtered from the Hilbert transform of the 405kyr cycle, the Hilbert transform of the 405kyr cycle and the band power of the 405kyr cycle / Total spectral power. In this case it indicates that the period of the 2.4 Myr cycle changes to a cycle with a 1.2

Myr duration which cannot be extracted with a filter centered on the 2.4 Myr cycle hence the apparent mismatch. The Astronomical features of the 1.2Myr Obliquity remain constant during both chaotic resonance transitions indicating the 1.2Myr Obliquity remained stable during this period.

5.2 Expression of astronomical cycles during Ocean Anoxic Event 2

Previous studies on low and middle paleolatitude records of OAEII contain a well expressed obliquity cycle especially during the latter part of OAEII (Charbonnier et al., 2018; Kuypers et al., 2004; Meyers et al., 2012). A well-expressed obliquity cycle can also be observed in this record (Figures 9 and 11). Whether the presence of and obliquity signal at low and middle paleolatitude during OAEII is related to processes acting due to the climatic perturbation which is OAEII or due to a change in the contribution of obliquity to the astronomical-insolation during OAEII remains unresolved. Obliquity can be present in low and middle paleolatitude records either due to a high latitude teleconnection such as the: formation of high latitude intermediate/deep-water formation transporting water from the poles to lower latitudes, an obliquity modulated meridional temperature gradient impacting low-latitude wind strength or the establishment of polar icecaps changing global climate patterns or due to a modulation of monsoonal activity by obliquity (Berrocoso et al., 2008; Bosmans et al., 2015; Friedrich et al., 2008; Kuhnt et al., 1997; März et al., 2009; Nederbragt et al., 2005). The amplitude modulation extracted from G17-S-01 in combination with the filtered 173 kyr obliquity and 405 kyr eccentricity cycles provides insights whether the strong obliquity signal during OAEII is related to processes acting due to the climatic perturbation which is OAEII or due to a relative increase of obliquity to the astronomical-insolation during OAEII (Figures 9 and 11.). In well G17-S-01 Th the 2.4 Myr eccentricity cycle and eccentricity spectral power peak just before OAEII and trends towards a minimum during OAEII while the 1.2 Myr obliquity cycle and obliquity spectral power reaches a minimum just before the onset of OAEII and increases during OAEII (Figure 11). The phase relationship between the 2.4 Myr eccentricity cycle and 1.2 Myr obliquity cycle indicates that during the latter part of OAEII, both the relative (2.4 Myr eccentricity decreasing) and absolute (a 1.2Myr obliquity maxima) contribution of obliquity to the astronomical-insolation increases, which should lead to a more pronounced expression of the obliquity cycle in the geological record during the latter part of OAEII. This progressive increase in the contribution of obliquity is astronomical-insolation agrees with the Tarfaya S13 and ODP1261B well records of Meyers et al. (2012a).

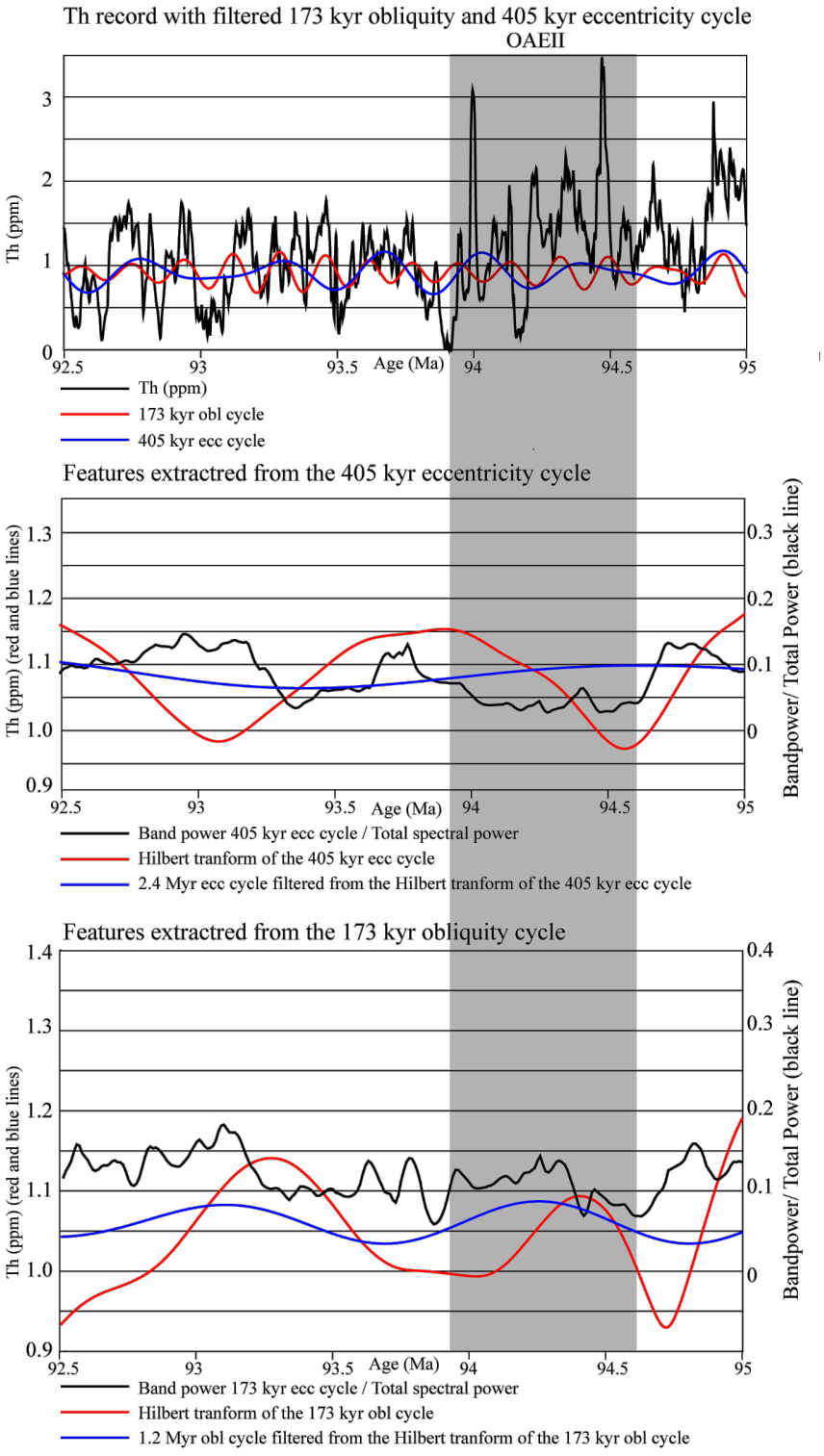
Th record with filtered 173 kyr obliquity and 405 kyr eccentricity cycle
OAEII
Th (ppm)
Age (Ma)
Th (ppm)
173 kyr obl cycle
405 kyr ecc cycle
Features extractred from the 405 kyr eccentricity cycle
Th (ppm) (red and blue lines)
Bandpower/ Total Power (black line)
Band power 405 kyr ecc cycle / Total spectral power
Hilbert tranform of the 405 kyr ecc cycle
2.4 Myr ecc cycle filtered from the Hilbert tranform of the 405 kyr ecc cycle
Features extractred from the 173 kyr obliquity cycle
Band power 173 kyr ecc cycle / Total spectral power
Hilbert tranform of the 173 kyr obl cycle
1.2 Myr obl cycle filtered from the Hilbert tranform of the 173 kyr obl cycle

Figure 11. The record Well-log G17-S-01 Th tuned to La2010d zoomed in to the 92 Ma to 95 Ma interval. The grey interval is OAEII. Top window Th log and the 173 kyr obl and 405 kyr ecc cycles. Middle window band power/total power for the 405 kyr ecc cycle, Hilbert transform of the 405 kyr ecc cycle and the 2.4 Myr ecc cycle filtered from the Hilbert transform. Bottom window band power/total power for the 173 kyr obl cycle, Hilbert transform of the 173 kyr ecc cycle and the 1.2 Myr obl cycle filtered from the Hilbert transform.

6. Conclusions

The Chalk Group on the Dutch Schill Grund platform represents a practically complete 30 Myr long stratigraphic record which contains the imprint of astronomical cycles. The record is converted from the depth to the time domain and is subsequently anchored to the astronomical solution of La2010d. The 30 Myr long record allowed the study of two facets of the expression of long astronomical cycles (>1 Myr period especially) during the late Cretaceous. First, the amplitude modulation of eccentricity and obliquity cycles in our record was compared the results of Ma et al., (2019, 2017) and exiting astronomical solutions. The 2.4 Myr eccentricity cycle extracted from Th log of well G17-S-01 confirms the findings of Ma et al., (2019, 2017) that a secular resonance transition took place at ~92 and ~985 Ma in which the period of the 2.4 Myr eccentricity cycle switched to a 1.2 Myr period between ~92Ma and ~85Ma. The amplitude modulation records extracted from the astronomical solutions does not fit with the amplitude modulation records extracted from the well-logs indicating that astronomical solutions do not accurately model the secular resonance state between the 1.2 Myr obliquity and 2.4 during the Late cretaceous. Secondly the imprint of astronomical cycles on OAEII was investigated. Astronomical cycles do modulate the geological record during OAEII, with the 2.4 Myr eccentricity reaching a maximum ~400kyr before OAEII and progressively declining during OAEII while the 1.2 Myr obliquity cycle is at a minimum just before OAEII and peaks during OAEII. The phase relationship between the 2.4 Myr eccentricity cycle and 1.2 Myr obliquity cycle indicates the contribution of obliquity to the astronomical-insolation progressively increased during OAEII, which explains the well-defined obliquity signal observed in this and other studies of low and middle paleolatitude records during the latter part of OAEII.

8. Acknowledgement

This Paper could not have been possible without the financial support of FNRS-PDR T.0051.19. Utrecht University and TNO-GDN are thanked for the time and money made available by the personnel to support this paper. The work has greatly benefited from discussion with of TNO-GDN personnel Dr. Dirk Munsterman Dr. Geert de Bruin, Stephan Carpentier and Dr. Johan ten Veen. TNO-GDN is also thanked for making the data-set available for this research.

This paper is a contribution to IGCP-652 “Reading geologic time in Paleozoic sedimentary rocks”.

9. References

Bachmann, G.H., Geluk, M.C., Warrington, G., Becker-Roman, A., Beutler, G., Hagdorn, H., Hounslow, M.W., Nitsch, E., Röhling, H.G., Simon, T., Szulc, A., 2010. Chapter 9 Triassic, in: Petroleum Geological Atlas of the Southern Permian Basin Area. pp. 149–173.Batenburg, S.J., 2013. Cyclostratigraphy and astronomical tuning of the Maastrichtian limestone-marl alternations at Zumaia and Sopelana, Basque country, N-Spain. Dr. Thesis Univ. Portsmouth 203.Batenburg, S.J., Gale, A.S., Sprovieri, M., Hilgen, F.J., Thibault, N., Boussaha, M., Orue-Etxebaria, X., Orue-Etxebarria, X., Orue-Etxebaria, X., 2014. An astronomical time scale for the Maastrichtian based on the Zumaia and Sopelana sections (Basque country, northern Spain). J. Geol. Soc. London. 171, 165–180. https://doi.org/10.1144/jgs2013-015Batenburg, S.J., Sprovieri, M., Gale, A.S., Hilgen, F.J., Hüsing, S.K., Laskar, J., Liebrand, D., Lirer, F., Orue-Etxebarria, X., Pelosi, N., Smit, J., 2012. Cyclostratigraphy and astronomical tuning of the Late Maastrichtian at Zumaia (Basque country, Northern Spain). Earth Planet. Sci. Lett. 359–360, 264–278. https://doi.org/10.1016/j.epsl.2012.09.054Berrocoso, Á.J., MacLeod, K.G., Calvert, S.E., Elorza, J., 2008. Bottom water anoxia, inoceramid colonization, and benthopelagic coupling during black shale deposition on Demerara Rise (Late Cretaceous western tropical North Atlantic). Paleoceanography 23. https://doi.org/10.1029/2007PA001545Bosmans, J.H.C., Hilgen, F.J., Tuenter, E., Lourens, L.J., 2015. Obliquity forcing of low-latitude climate. Clim. Past 11, 1335–1346. https://doi.org/10.5194/cp-11-1335-2015Boussaha, M., Thibault, N., Stemmerik, L., 2016. Integrated stratigraphy of the late Campanian – Maastrichtian in the Danish Basin: revision of the Boreal calcareous nannofossil zonation. Newsletters Stratigr. 49, 337–360. https://doi.org/10.1127/nos/2016/0075C. Gouhier, T., Grinsted, A., Simko, V., 2019. Package ‘biwavelet.’Charbonnier, G., Boulila, S., Spangenberg, J.E., Adatte, T., Föllmi, K.B., Laskar, J., 2018. Obliquity pacing of the hydrological cycle during the Oceanic Anoxic Event 2. Earth Planet. Sci. Lett. 499, 266–277. https://doi.org/10.1016/j.epsl.2018.07.029Clarkson, M.O., Stirling, C.H., Jenkyns, H.C., Dickson, A.J., Porcelli, D., Moy, C.M., Von Strandmann, P.P.A.E., Cooke, I.R., Lenton, T.M., 2018. Uranium isotope evidence for two episodes of deoxygenation during Oceanic Anoxic Event 2. Proc. Natl. Acad. Sci. U. S. A. 115, 2918–2923. https://doi.org/10.1073/pnas.1715278115Damholt, T., Surlyk, F., 2004. Laminated-bioturbated cycles in Maastrichtian chalk of the North Sea: Oxygenation fluctuations within the Milankovitch frequency band. Sedimentology 51, 1323–1342. https://doi.org/10.1111/j.1365-3091.2004.00672.xDanzelle, J., Riquier, L., Baudin, F., Thomazo, C., Pucéat, E., 2018. Oscillating redox conditions in the Vocontian Basin (SE France)

during Oceanic Anoxic Event 2 (OAE 2). Chem. Geol. 493, 136–152. https://doi.org/10.1016/j.chemgeo.2018.05.039De Jager, J., 2007. Geological development, in: Geology of the Netherlands Edited by Th.E.Wong, D.A.J. Batjes & J. de Jager Royal Netherlands Academy of Arts and Sciences, 2007. pp. 5–26.De Vos, W., Feldrappe, H., Pharaoh, T.C., Smith, N.J.P., Vejbæk, O.V., Verniers, J., Nawrocki, J., Poprawa, P., Bełka, Z., 2010. Chapter 4 Pre-Devonian, in: Petroleum Geological Atlas of the Southern Permian Basin Area. pp. 58–69.Ellis, D. V, Singer, J.M., 2007. Well Logging for Earth Scientists. https://doi.org/10.1007/978-1-4020-4602-5Esmerode, E. V., Lykke-Andersen, H., Surlyk, F., 2008. Interaction between bottom currents and slope failure in the Late Cretaceous of the southern Danish Central Graben, North Sea. J. Geol. Soc. London. 165, 55–72. https://doi.org/10.1144/0016-76492006-138Esmerode, E. V., Lykke-Andersen, H., Surlyk, F., 2007. Ridge and valley systems in the Upper Cretaceous chalk of the Danish Basin: contourites in an epeiric sea. Geol. Soc. London, Spec. Publ. 276, 265–282. https://doi.org/10.1144/GSL.SP.2007.276.01.13Esmerode, E. V., Surlyk, F., 2009. Origin of channel systems in the Upper Cretaceous Chalk Group of the Paris Basin. Mar. Pet. Geol. 26, 1338–1349. https://doi.org/10.1016/j.marpetgeo.2009.05.001Friedrich, O., Batenburg, S.J., Moriya, K., Voigt, S., Cournède, C., Möbius, I., Blum, P., Bornemann, A., Fiebig, J., Hasegawa, T., Hull, P.M., Norris, R.D., Röhl, U., Westerhold, T., Wilson, P.A., IODP Expedition, 2016. Maastrichtian carbon isotope stratigraphy and cyclostratigraphy of the Newfoundland Margin (Site U1403, IODP Leg 342). Clim. Past Discuss. 1–21. https://doi.org/10.5194/cp-2016-51Friedrich, O., Norris, R.D., Bornemann, A., Beckmann, B., Pälike, H., Worstell, P., Hofmann, P., Wagner, T., 2008. Cyclic changes in Turonian to Coniacian planktic foraminiferal assemblages from the tropical Atlantic Ocean. Mar. Micropaleontol. 68, 299–313. https://doi.org/10.1016/j.marmicro.2008.06.003Geluk, M.C., 2007. Permian, in: Geology of the Netherlands Edited by Th.E.Wong, D.A.J. Batjes & J. de Jager Royal Netherlands Academy of Arts and Sciences, 2007. pp. 63–83.Geluk, M.M.C., 2007. Triassic, in: Geology of the Netherlands Edited by Th.E.Wong, D.A.J. Batjes & J. de Jager Royal Netherlands Academy of Arts and Sciences, 2007. pp. 85–106.Gennaro, M., Wonham, J.P., 2014. Channel development in the chalk of the Tor Formation, North Sea: Evidence of bottom current activity, in: From Depositional Systems to Sedimentary Successions on the Norwegian Continental Margin. pp. 551–586. https://doi.org/10.1002/9781118920435.ch19Hampton, M.J., Bailey, H.W., Gallanger, L.T., Mortimore, R.N., Wood, C.J., 2007. The biostratigraphy of Seaford Head, Sussex, southern England; an international reference section for the basal boundaries for the Santonian and Campanian Stages in chalk facies. Cretac. Res. 28, 46–60. https://doi.org/10.1016/j.cretres.2006.05.025Herbert, T.D., Fischer, A.G., 1986. Milankovitch climatic origin of mid-Cretaceous black shale rhythms in central Italy. Nature 321, 739–743. https://doi.org/10.1038/321739a0Herngreen, G.F.W., Wong, T.E., 2007. Cretaceous, in: Geology of the Netherlands Edited by Th.E.Wong, D.A.J. Batjes & J. de Jager Royal Netherlands

Academy of Arts and Sciences, 2007. pp. 127–150.Hilgen, F., Zeeden, C., Laskar, J., 2020. Paleoclimate records reveal elusive ~200-kyr eccentricity cycle for the first time. Glob. Planet. Change 194, 103296. https://doi.org/10.1016/j.gloplacha.2020.103296Hinnov, L.A., 2000. New Perspectives on Orbitally Forced Stratigraphy. Annu. Rev. Earth Planet. Sci. 28, 419–475. https://doi.org/10.1177/0741713604268894Huang, C., 2018. Astronomical Time Scale for the Mesozoic, Stratigraphy & Timescales. Elsevier Ltd. https://doi.org/10.1016/bs.sats.2018.08.005Husson, D., Galbrun, B., Laskar, J., Hinnov, L.A., Thibault, N., Gardin, S., Locklair, R.E., 2011. Astronomical calibration of the Maastrichtian (Late Cretaceous). Earth Planet. Sci. Lett. 305, 328–340. https://doi.org/10.1016/j.epsl.2011.03.008Jarvis, I., 1980. the Initiation of Phosphatic Chalk Sedimentation the Senonian Cretaceous of the Anglo Paris Basin. SEPM Spec. Publ. 167–192.Jenkyns, H.C., 2010. Geochemistry of oceanic anoxic events. Geochemistry, Geophys. Geosystems 11, 1–30. https://doi.org/10.1029/2009GC002788Jenkyns, H.C., 1999. Mesozoic anoxic events and palaeoclimate. Zentralblatt für Geol. und Paläontologie 7–9, 943–949.Knox, R.W.O.B., Bosch, J.H.A., Rasmussen, E.S., Heilmann-Clausen, C., Hiss, M., de Lugt, I.R., Kasiński, J.R., King, C., Köthe, A., Slodkowska, B., Standke, G., Vandenberghe, N., 2008. Chapter 12 Cenozoic. Pet. Geol. Atlas South. Permian Basin Area 211–223.Kombrink, H., Besly, B.M., Collinson, J.D., Den Hartog Jager, D.G. Drozdzewski, G., Dusar, M., Hoth, P., Pagnier, H.J.M., Stemmerik, L. Waksmundzka, M.I. Wrede, V., 2010. Chapter 6 Carboniferous, in: Petroleum Geological Atlas of the Southern Permian Basin Area. pp. 81–99.Kombrink, H., Doornenbal, J.C., Duin, E.J.T., den Dulk, M., ten Veen, J.H., Witmans, N., 2012. New insights into the geological structure of the Netherlands; results of a detailed mapping project. Netherlands J. Geosci. - Geol. en Mijnb. 91, 419–446. https://doi.org/10.1017/S0016774600000329Kuhnt, W., Nederbragt, A., Leine, L., 1997. Cyclicity of Cenomanian-Turonian organic-carbon-rich sediments in the Tarfaya Atlantic Coastal Basin (Morocco). Cretac. Res. 18, 587–601. https://doi.org/10.1006/cres.1997.0076Kuypers, M.M.M., Lourens, L.J., Rijpstra, W.I.C., Pancost, R.D., Nijenhuis, I.A., Sinninghe Damsté, J.S., 2004. Orbital forcing of organic carbon burial in the proto-North Atlantic during oceanic anoxic event 2. Earth Planet. Sci. Lett. 228, 465–482. https://doi.org/10.1016/j.epsl.2004.09.037Laskar, J., 1999. The limits of Earth orbital calculations for geological time-scale use. Philos. Trans. R. Soc. A Math. Phys. Eng. Sci. 357, 1735–1759. https://doi.org/10.1098/rsta.1999.0399Laskar, J., Fienga, A., Gastineau, M., Manche, H., 2011. La2010: A new orbital solution for the long-term motion of the Earth. Astron. Astrophys. 532. https://doi.org/10.1051/0004-6361/201116836Laskar, Jacques, Fienga, A., Gastineau, M., Manche, H., 2011a. La2010: A new orbital solution for the long term motion of the Earth. Astron. Astrophys. 4, 17. https://doi.org/10.1051/0004-6361/201116836Laskar, Jacques, Gastineau, M., Delisle, J.-B., Farrés, A., Fienga, A., 2011b. Strong chaos induced by close encounters with Ceres and Vesta. Astron. Astrophys. 532, L4. https://doi.org/10.1051/0004-6361/201117504Laskar, J., Robutel,

P., Joutel, F., Gastineau, M., Correia, a. C.M., Levrard, B., 2004. A long-term numerical solution for the insolation quantities of the Earth. Astron. Astrophys. 428, 261–285. https://doi.org/10.1051/0004-6361:20041335Laurin, J., Meyers, S.R., Galeotti, S., Lanci, L., Laurin, J., Meyers, S.R., Galeotti, S., Lanci, L., Laurin, J., Meyers, S.R., Galeotti, S., Lanci, L., 2016. Frequency modulation reveals the phasing of orbital eccentricity during Cretaceous Oceanic Anoxic Event II and the Eocene hyperthermals. Earth Planet. Sci. Lett. 442, 143–156. https://doi.org/10.1016/j.epsl.2016.02.047Lenniger, M., Nøhr-Hansen, H., Hills, L. V., Bjerrum, C.J., 2014. Arctic black shale formation during Cretaceous Oceanic Anoxic event 2. Geology 42, 799–802. https://doi.org/10.1130/G35732.1Liebrand, D., Raffi, I., Fraguas, Á., Laxenaire, R., Bosmans, J.H.C., Hilgen, F.J., Wilson, P.A., Batenburg, S.J., Beddow, H.M., Bohaty, S.M., Bown, P.R., Crocker, A.J., Huck, C.E., Lourens, L.J., Sabia, L., 2018. Orbitally Forced Hyperstratification of the Oligocene South Atlantic Ocean. Paleoceanogr. Paleoclimatology 33, 511–529. https://doi.org/10.1002/2017PA003222Lykke-Andersen, H., Surlyk, F., 2004. The Cretaceous-Palaeogene boundary at Stevns Klint, Denmark: inversion tectonics or sea-floor topography? J. Geol. Soc. London. 161, 343–352. https://doi.org/10.1144/0016-764903-021Ma, C., Meyers, S.R., Sageman, B.B., 2019. Testing Late Cretaceous astronomical solutions in a 15 million year astrochronologic record from North America. Earth Planet. Sci. Lett. 513, 1–11. https://doi.org/10.1016/j.epsl.2019.01.053Ma, C., Meyers, S.R., Sageman, B.B., 2017. Theory of chaotic orbital variations confirmed by Cretaceous geological evidence. Lett. to Nat. 542, 468–470. https://doi.org/10.1038/nature21402März, C., Beckmann, B., Franke, C., Vogt, C., Wagner, T., Kasten, S., 2009. Geochemical environment of the Coniacian-Santonian western tropical Atlantic at Demerara Rise. Palaeogeogr. Palaeoclimatol. Palaeoecol. 273, 286–301. https://doi.org/10.1016/j.palaeo.2008.05.004Meyers, S.R., 2014. Astrochron: An R Package for AstrochronologyNo Title.Meyers, S.R., 2012. Seeing red in cyclic stratigraphy: Spectral noise estimation for astrochronology. Paleoceanography 27, 1–12. https://doi.org/10.1029/2012PA002307Meyers, S.R., Sageman, B.B., 2007. Quantification of deep-time orbital forcing by average spectral misfit. Am. J. Sci. 307, 773–792. https://doi.org/10.2475/05.2007.01Meyers, S.R., Sageman, B.B., Arthur, M.A., 2012. Obliquity forcing of organic matter accumulation during Oceanic Anoxic Event 2. Paleoceanography 27, 1–19. https://doi.org/10.1029/2012PA002286Nederbragt, A.J., Thurow, J., Pearce, R., 2005. Sediment composition and cyclicity in the Mid-Cretaceous at Demerara Rise, ODP Leg 207. Proc. Ocean Drill. Progr. Sci. Results 207. https://doi.org/10.2973/odp.proc.sr.207.103.2007Niebuhr, B., Prokoph, A., 1997. Periodic-cyclic and chaotic successions of Upper Cretaceous (Cenomanian to Campanian) pelagic sediments in the North German Basin. Cretac. Res. 18, 731–750. https://doi.org/10.1006/cres.1997.0083Niebuhr, B., Wiese, F., Wilmsen, M., 2001. The cored konrad 101 borehole (Cenomanian-Lower coniacian, lower saxony): Calibration of surface and subsurface log data for the lower upper cretaceous of northern Germany. Cretac. Res. 22, 643–674. https://doi.org/10.1006/cres.2001.0283Olsen, P.E., Laskar, J., Kent, D. V.,

Kinney, S.T., Reynolds, D.J., Sha, J., Whiteside, J.H., 2019. Mapping solar system chaos with the geological orrery. Proc. Natl. Acad. Sci. U. S. A. 166, 10664–10673. https://doi.org/10.1073/pnas.1813901116Pearce, M.A., Jarvis, I., Ball, P.J., Laurin, J., 2020. Palynology of the Cenomanian to lowermost Campanian (Upper Cretaceous) Chalk of the Trunch Borehole (Norfolk, UK) and a new dinoflagellate cyst bioevent stratigraphy for NW Europe. Rev. Palaeobot. Palynol. 278. https://doi.org/10.1016/j.revpalbo.2020.104188Perdiou, A., Thibault, N., Anderskouv, K., van Buchem, F., Arie, B., Joan, G., Bjerrum, C.J., 2015. Orbital calibration of the late Campanian carbon isotope event in the North Sea. J. Geol. Soc. London. 173, 2015–120. https://doi.org/10.1144/jgs2015-120Pharaoh, T., Dusar, M., Geluk, M., Kockel, F., Krawczyk, Charlotte Krzywiec, P., Scheck-Wenderoth, M., Hans, T., Vejbæk, O.V., Wees, J.D. Van, 2003. Chapter 3 Tectonic evolution, in: Petroleum Geological Atlas of the Southern Permian Basin Area. pp. 25–57.R Core Team, 2020. R: A language and environment for statistical computing. R Foundation for Statistical Computing, Vienna, Austria. URL https://www.R-project.org/.Remin, Z., Gruszczyński, M., Marshall, J.D., Gruszczy??ski, M., Marshall, J.D., 2016. Changes in paleo-circulation and the distribution of ammonite faunas at the Coniacian–Santonian transition in central Poland and western Ukraine. Acta Geol. Pol. 66, 107–124. https://doi.org/10.1515/agp-2016-0006Ruddiman, W.F., 2008. Earth's climate: past and future by. https://doi.org/10.1016/S0921-8181(01)00108-4Schlanger, S.O., Arthur, M.. M.A., Jenkyns, H.C., Scholle, P.A.P.A.A., 1987. The Cenomanian Turonian oceanic anoxic event I . Stratigraphy and distribution of organic carbon rich beds and the C13 excursion. Mar. Pet. Source Rocks Geol. Soc. Spec. Publ. 26, 371–399. https://doi.org/10.1144/GSL.SP.1987.026.01.24Schlanger, S.O., Jenkyns, H.C., 1976. Cretaceous Oceanic Anoxic Events: Causes and Consequences. Geol. en Mijnb.Surlyk, F., Jensen, S.K., Engkilde, M., 2008. Deep channels in the Cenomanian-Danian chalk group of the German North sea sector: Evidence of strong constructural and erosional bottom currents and effect on reservoir quality distribution. Am. Assoc. Pet. Geol. Bull. 92, 1565–1586. https://doi.org/10.1306/07100808035Surlyk, F., Lykke-Andersen, H., 2007. Contourite drifts, moats and channels in the Upper Cretaceous chalk of the Danish Basin. Sedimentology 54, 405–422. https://doi.org/10.1111/j.1365-3091.2006.00842.xTakashima, R., Nishi, H., Huber, B., Leckie, R.M., 2006. Greenhouse World and the Mesozoic Ocean. Oceanography 19, 82–92. https://doi.org/10.5670/oceanog.2006.07Ten Veen, J.H., Postma, G., 1996. Astronomically forced variations in gamma-ray intensity: Late Miocene hemipelagic successions in the eastern Mediterranean basin as a test case. Geology 24, 15–18. https://doi.org/10.1130/0091-7613(1996)024<0015:AFVIGR>2.3.CO;2Ten Veen, J.H., Van Gessel, S.F., Den Dulk, M., 2012. Thin-and thick-skinned salt tectonics in the Netherlands; A quantitative approach. Netherlands J. Geosci. Geol. en Mijnb. 91, 447–464. https://doi.org/10.1017/S0016774600000330Thomson, D.J., 1982. Spectrum estimation and harmonic analysis. Proc. IEEE 70, 1055–1096. https://doi.org/10.1109/PROC.1982.12433TNO-GDN, 2022. Stratigrafische

Nomenclator van Nederland, TNO – Geologische Dienst Nederland. [WWW Document]. http://www.dinoloket.nl/stratigrafische-nomenclator.TNO, 2011. Tectono-stratigraphic Charts of the Netherlands Continental Shelf.Trabucho Alexandre, J.P., Tuenter, E., Henstra, G.A., Van Der Zwan, K.J., Van De Wal, R.S.W., Dijkstra, H.A., De Boer, P.L., 2010. The mid-Cretaceous North Atlantic nutrient trap: Black shales and OAEs. Paleoceanography 25, 1–14. https://doi.org/10.1029/2010PA001925van Adrichem Boogaert, H.A., Kouwe, W.F.P., 1994. Stratigraphic nomenclature of the Netherlands, revision and updat by RGD and NOGEPA. Medelingen Rijks Geol. D. 50.van Buggenum, J.M., Den Hartog Jager, D.G., 2007. Silesian, in: Geology of the Netherlands Edited by Th.E.Wong, D.A.J. Batjes & J. de Jager Royal Netherlands Academy of Arts and Sciences, 2007. pp. 43–62.Van der Molen, A.S., 2004. Sedimentary development, seismic stratigraphy and burial compaction of the Chalk Group in the Netherlands North Sea area. Geol. ULTRAIECTINA.Van der Voet, E., 2015. Geological evolution of the Chalk Group in the northern Dutch North Sea. MSc. thesis VU Amsterdam 104.Vejbæk, O.V., Andersen, C., Dusar, M., Herngreen, G.F.W., Krabbe, H., Leszczyński, K., Lott, G.K., Mutterlose, J., Van der Molen, A.S., Hergreen, W., Krabbe, H., Leszcynski, K., Valdemar, O., Hess, V., Aps, D., Geus, C.A., Gsb, M.D., Herngreen, W., 2010. Chapter 11 Cretaceous, in: Petroleum Geological Atlas of the Southern Permian Basin Area. pp. 195–209.Voigt, S., Schönfeld, J., 2010. Cyclostratigraphy of the reference section for the Cretaceous white chalk of northern Germany, Lägerdorf-Kronsmoor: A late Campanian-early Maastrichtian orbital time scale. Palaeogeogr. Palaeoclimatol. Palaeoecol. 287, 67–80. https://doi.org/10.1016/j.palaeo.2010.01.017Westerhold, T., Röhl, U., Laskar, J., 2012. Time scale controversy: Accurate orbital calibration of the early Paleogene. Geochemistry, Geophys. Geosystems 13, 1–19. https://doi.org/10.1029/2012GC004096Westerhold, T., Röhl, U., Raffi, I., Fornaciari, E., Monechi, S., Reale, V., Bowles, J., Evans, H.F., 2008. Astronomical calibration of the Paleocene time. Palaeogeogr. Palaeoclimatol. Palaeoecol. 257, 377–403. https://doi.org/10.1016/j.palaeo.2007.09.016Wong, T.E., de Lugt, I.R., Kuhlmann, G., Overeem, I., 2007. Tertiary, in: Geology of the Netherlands Edited by Th.E.Wong, D.A.J. Batjes & J. de Jager Royal Netherlands Academy of Arts and Sciences, 2007. pp. 151–171.Wong, T.E., Dusar, M., Andsbjerg, J., Mönnig, E., Feldman-Olszewska, A., Verreussel, R.M.C.H., 2010. Chapter 10 Jurassic. Pet. Geol. Atlas South. Permian Basin Area 175–193.Worthington, P.F., 1990. Sediment cyclicity from well logs. Geol. Soc. London, Spec. Publ. 48, 123–132. https://doi.org/10.1144/GSL.SP.1990.048.01.11Wu, H., Zhang, S., Hinnov, L.A., Jiang, G., Yang, T., Li, H., Wan, X., Wang, C., 2014. Cyclostratigraphy and orbital tuning of the terrestrial upper Santonian-Lower Danian in Songliao Basin, northeastern China. Earth Planet. Sci. Lett. 407, 82–95. https://doi.org/10.1016/j.epsl.2014.09.038Wu, H., Zhang, S., Jiang, G., Hinnov, L.A., Yang, T., Li, H., Wan, X., Wang, C., 2013. Astrochronology of the Early Turonian-Early Campanian terrestrial succession in the Songliao Basin, northeastern China and its implication for long-period behavior of

the Solar System. Palaeogeogr. Palaeoclimatol. Palaeoecol. 385, 55–70. https://doi.org/10.1016/j.palaeo.2012.09.004Zijlstra, J.J.P., 1994. Sedimentology of the Late Cretaceous and Early Tertiary (Tuffaceous) Chalk of the Northwest Europe. Meded. van Fac. Aardwetenschappen Univ. Utr. 119, 1–192.

References from the Supporting Information

Batenburg, S. J. (2013). Cyclostratigraphy and astronomical tuning of the Maastrichtian limestone-marl alternations at Zumaia and Sopelana, Basque country, N-Spain. Doctoral Thesis University of Portsmouth, 203.

Batenburg, S. J., Sprovieri, M., Gale, A. S., Hilgen, F. J., Hüsing, S. K., Laskar, J., et al. (2012). Cyclostratigraphy and astronomical tuning of the Late Maastrichtian at Zumaia (Basque country, Northern Spain). Earth and Planetary Science Letters, 359–360(October 2019), 264–278. https://doi.org/10.1016/j.epsl.2012.09.054

Batenburg, S. J., Gale, A. S., Sprovieri, M., Hilgen, F. J., Thibault, N., Boussaha, M., et al. (2014). An astronomical time scale for the Maastrichtian based on the Zumaia and Sopelana sections (Basque country, northern Spain). Journal of the Geological Society, 171(2), 165–180. https://doi.org/10.1144/jgs2013-015

Friedrich, O., Batenburg, S. J., Moriya, K., Voigt, S., Cournède, C., Möbius, I., et al. (2016). Maastrichtian carbon isotope stratigraphy and cyclostratigraphy of the Newfoundland Margin (Site U1403, IODP Leg 342). Climate of the Past Discussions, (May), 1–21. https://doi.org/10.5194/cp-2016-51

Gale, A. S., Mutterlose, J., Batenburg, S., Gradstein, F. M., Agterberg, F. P., Ogg, J. G., & Petrizzo, M. R. (2020). Chapter 27 - The Cretaceous Period. In F. M. Gradstein, J. G. Ogg, M. D. Schmitz, & G. M. Ogg (Eds.), Geologic Time Scale 2020 (pp. 1023–1086). Elsevier. https://doi.org/https://doi.org/10.1016/B978-0-12-824360-2.00027-9

Gradstein, F. M., Waters, C. N., Charnock, M., Munsterman, D., Hollerbach, M., Brunstad, H., et al. (2016). Stratigraphic Guide to the Cromer Knoll, Shetland and Chalk Groups, North Sea and Norwegian Sea. Newsletters on Stratigraphy, 49(1), 71–280. https://doi.org/10.1127/nos/2016/0071

Hardenbol, J., Thierry, J., Farley, M. B., Jacquin, T., De Graciansky, P.-C., & Vail, P. R. (1998a). Appendix: Mesozoic and Cenozoic Sequence Chronostratigraphic Framework of European Basins. SEPM Special Publication, (60), 763–786. https://doi.org/10.2110/pec.98.02.0003

Hardenbol, J., Thierry, J., Farley, M. B., Jacquin, T., De Graciansky, P.-C., & Vail, P. R. (1998b). Mesozoic and Cenozoic Sequence Stratigraphy of European Basins. SEPM Special Publications, 60(60), 3–13. https://doi.org/10.2110/pec.98.02.0003

Husson, D., Galbrun, B., Laskar, J., Hinnov, L. A., Thibault, N., Gardin, S., & Locklair, R. E. (2011). Astronomical calibration of the Maastrichtian

(Late Cretaceous). Earth and Planetary Science Letters, 305(3–4), 328–340. https://doi.org/10.1016/j.epsl.2011.03.008

Ma, C., Meyers, S. R., & Sageman, B. B. (2017). Theory of chaotic orbital variations confirmed by Cretaceous geological evidence. Letters to Nature, 542(7642), 468–470. https://doi.org/10.1038/nature21402

Sikora, P. J., Bergen, J. a., & Farmer, C. L. (1999). Chalk palaeoenvironments and depositional model, Valhall-Hod fields, southern Norwegian North Sea. Geological Society, London, Special Publications, 152, 113–137. https://doi.org/10.1144/GSL.SP.1999.152.01.07

Westerhold, T., Röhl, U., Raffi, I., Fornaciari, E., Monechi, S., Reale, V., et al. (2008). Astronomical calibration of the Paleocene time. Palaeogeography, Palaeoclimatology, Palaeoecology, 257(4), 377–403. https://doi.org/10.1016/j.palaeo.2007.09.016

Wu, H., Zhang, S., Hinnov, L. A., Jiang, G., Yang, T., Li, H., et al. (2014). Cyclostratigraphy and orbital tuning of the terrestrial upper Santonian-Lower Danian in Songliao Basin, northeastern China. Earth and Planetary Science Letters, 407, 82–95. https://doi.org/10.1016/j.epsl.2014.09.038

Data Availability Statement

All used data is available for download from NLOG the Dutch Oil and Gas portal datacentre (https://www.nlog.nl/datacenter). Data with regards to borehole measurements and metadata is available on (https://www.nlog.nl/datacenter /brh-overview). All seismic data including survey information and the seismic data itself can be downloaded from (https://www.nlog.nl/datacenter/smc-lines)